---

**Article:**
Willis, A.P., Kerswell, R.R. and Pringle, C.C.T. (2014) An optimization approach for analysing nonlinear stability with transition to turbulence in fluids as an exemplar. Reports on Progress in Physics, 77. 085901. ISSN 1361-6633

https://doi.org/10.1088/0034-4885/77/8/085901

---

REVIEW ARTICLE

# An optimisation approach for analysing nonlinear stability with transition to turbulence in fluids as an exemplar

**R R Kerswell[1], C C T Pringle[2] and A P Willis[3]**

[1] School of Mathematics, University of Bristol, Bristol BS8 1TW, UK
[2] Applied Mathematics Research Centre, Faculty of Engineering and Computing, Coventry University, Coventry CV1 5FB, UK
[3] School of Mathematics and Statistics, University of Sheffield, Sheffield S3 7RH, UK

E-mail: R.R.Kerswell@bris.ac.uk

DRAFT: 5 February 2014

**Abstract.**

This article introduces, and reviews recent work using, a simple optimisation technique for analysing the nonlinear stability of a state in a dynamical system. The technique can be used to identify the most efficient way to disturb a system such that it transits from one stable state to another. The key idea is introduced within the framework of a finite-dimensional set of ordinary differential equations (ODEs) and then illustrated for a very simple system of 2 ODEs which possesses bistability. Then the transition to turbulence problem in fluid mechanics is used to show how the technique can be formulated for a spatially-extended system described by a partial differential equation (the well-known Navier-Stokes equation). Within that context, the optimisation technique bridges the gap between (linear) optimal perturbation theory and the (nonlinear) dynamical systems approach to fluid flows. The fact that the technique has now been recently shown to work in this very high dimensional setting augers well for its utility in other physical systems.

PACS numbers:

## 1. Introduction

Many physical systems possess a multiplicity of stable states so that more than one solution or system configuration can be found at long times. In such situations, a key issue is usually maintaining the system in a desired state against ambient noise or switching the system from one (undesirable) state to another (preferred) state in an efficient, robust way: e.g. in liquid crystal displays [61], power grids [71], arrays of coupled lasers [37], turbulent fluid flows [46] and even in the human brain [3]. Either objective involves detailed knowledge of a state's basin of attraction, defined as the set of all initial conditions of the system whose long time behaviour is to converge to that state. Initial conditions located just outside the basin boundary determine how the system can be efficiently disturbed to trigger a new stable state. Knowledge of how the basin boundary of a state moves (in phase space) when the system is manipulated (e.g. by modifying the boundary conditions) opens up the possibility of enhancing the nonlinear stability of that state. However, locating a basin boundary is a fully nonlinear (nonlocal) problem so that the traditional tools of linearising the system around the state or even weakly nonlinear analysis provide no traction. Existing fully nonlinear approaches - solving the governing equations while searching for the finite-amplitude disturbances to just knock the system out of one state into another, or mapping out the stable and unstable manifolds of nearby solutions in phase space to identify the basin boundary - are impractical for all but the smallest systems.

Recently, a new, very general, fully nonlinear optimisation technique has emerged as a viable way to make progress. The underlying idea is relatively simple and, perhaps because of this, seems to have been formulated independently in (at least) three different parts of the scientific literature over the last decade (transitional shear flows [18, 73, 86] - see §3, oceanography [76] - see §4.1 and thermoacoustics [62] - see §4.2). The key advance, however, has come in the last few years when the feasibility of the approach has been demonstrated for the 3-dimensional Navier-Stokes equations discretised by a large number ($O(10^5$-$10^6)$) of degrees of freedom [18, 19, 21, 33, 73, 86, 87, 89]. This suggests that other partial differential equation systems could be usefully analysed with this approach.

This article (which is an updated and extended version of [59]) is an attempt to provide a simple introduction to the idea and to review the progress made so far. As should become clear, the approach is still developing but there is already enough evidence garnered to indicate that it adds something quite new to a theoretician's toolbox. In fluid mechanics, the last two decades have seen a huge amount of work looking at flow transition either from the linear transient growth perspective (also called 'non-modal analysis' or 'optimal perturbation theory' [46, 94, 98, 97]) or more recently in terms of exact solutions and their manifolds (a dynamical systems approach [58, 35, 57]). The optimisation technique discussed here bridges the well-known 'amplitude' gap between these two viewpoints by extending the (infinitesimal amplitude) transient growth optimal of the former approach into finite amplitudes and ultimately up to where

the basin boundary is crossed (the closest stable manifold of a nearby exact solution).

The plan of this article is as follows. In section 2, the central idea of the optimisation approach is introduced in the context of a finite-dimensional dynamical system. A simple system of 2 ordinary differential equations (ODEs) is then used to: a) illustrate the results of a calculation, and b) highlight some important ingredients which make the technique work. In section 3, the discussion is moved onto fluid mechanics and the Navier-Stokes equation - a time-dependent and 3-space dimension nonlinear partial differential equation (PDE). The first attempted use of the optimisation technique was in the classical problem of flow through a pipe [86] and so this is used here as the context to explain the inner workings of the approach. Appendices A and B provide simple supporting illustrations of a linear transient growth calculation for a system of 2 ODEs and how including nonlinearity can allow different growth mechanisms to work together to produce far greater overall growth. Section 4 reviews some of the literature which preceded the successful application to the Navier-Stokes equations as well as discussing further work now building on it. Finally section 5 provides a summary and surveys what the future may hold.

## 2. Basic Idea

To explain the optimisation technique, consider a finite-dimensional dynamical system

$$\frac{d\mathbf{X}}{dt} = \mathbf{f}(\mathbf{X}; \mu) \tag{1}$$

where $\mathbf{X} = \mathbf{X}(t) \in \mathbb{R}^N$ and $\mu$ is a parameter of the system. Let $\mathbf{X}_0$ be a local steady attractor of interest and $\mathbf{x} := \mathbf{X} - \mathbf{X}_0$ be the perturbation away from this attractor. Then write the evolution equation for $\mathbf{x}$ as

$$\frac{d\mathbf{x}}{dt} = \mathbf{F}(\mathbf{x}; \mathbf{X}_0, \mu) \tag{2}$$

and define a norm $\|\mathbf{x}(t)\|$ to measure the distance of $\mathbf{X}(t)$ from $\mathbf{X}_0$. The approach is to find the maximum distance after some time $t = T$, $\|\mathbf{x}(T)\|$, over all perturbations which start the same finite distance

$$\|\mathbf{x}(0)\| = d \tag{3}$$

away at time $t = 0$ and evolve under (2). For the Euclidean norm, $\|\mathbf{x}\|_2 := \sqrt{\sum_{n=1}^{N} x_i^2}$, this can be formulated particularly easily as maximising the Lagrangian

$$\mathcal{L} = \mathcal{L}(\mathbf{x}, \boldsymbol{\nu}, \lambda; \mathbf{X}_0, d, T) := \|\mathbf{x}(T)\|_2^2 + \int_0^T \boldsymbol{\nu}.\Big(\frac{d\mathbf{x}}{dt} - \mathbf{F}\Big)\, dt + \lambda(\|\mathbf{x}(0)\|_2^2 - d^2) \tag{4}$$

with $\boldsymbol{\nu}(t)$ and $\lambda$ acting as Lagrange multipliers to impose the dynamical constraint (2) and initial distance constraint respectively and '.' is the usual scalar product. Maximal values of $\mathcal{L}$ are identified by vanishing first variations with respect to each of $\mathbf{x}(t)$, $\boldsymbol{\nu}(t)$ and $\lambda$ ( $\mathbf{X}_0$, $d$ and $T$ are fixed ). The first variation of $\mathcal{L}$ with respect to $\mathbf{x}(t)$ is

$$\delta\mathcal{L} \quad := \lim_{\epsilon \to 0} \frac{\mathcal{L}(\mathbf{x} + \epsilon\delta\mathbf{x}, \boldsymbol{\nu}, \lambda; \mathbf{X}_0, d, T) - \mathcal{L}(\mathbf{x}, \boldsymbol{\nu}, \lambda; \mathbf{X}_0, d, T)}{\epsilon}$$

$$= \left[\, 2\mathbf{x}(T) + \boldsymbol{\nu}(T) \,\right] \cdot \delta\mathbf{x}(T) - \int_0^T \left[ \frac{d\boldsymbol{\nu}}{dt} + \boldsymbol{\nu} \cdot \frac{\partial \mathbf{F}}{\partial \mathbf{x}} \right] \cdot \delta\mathbf{x}\, dt + \left[\, 2\lambda\mathbf{x}(0) - \boldsymbol{\nu}(0) \,\right] \cdot \delta\mathbf{x}(0) \qquad (5)$$

which only vanishes for all allowed variations $\delta\mathbf{x}(t)$ if

$$\frac{d\boldsymbol{\nu}}{dt} + \boldsymbol{\nu} \cdot \frac{\partial \mathbf{F}}{\partial \mathbf{x}} = \mathbf{0} \qquad \text{over } t \in (0, T) \qquad (6)$$

*and*

$$2\lambda\mathbf{x}(0) - \boldsymbol{\nu}(0) = 2\mathbf{x}(T) + \boldsymbol{\nu}(T) = 0. \qquad (7)$$

Stationarity of $\mathcal{L}$ with respect to the Lagrange multipliers $\boldsymbol{\nu}$ and $\lambda$ by construction imposes the evolution equation (2) and the initial distance constraint (3) respectively. Maximising $\mathcal{L}$ is then a problem of simultaneously satisfying (2), (3), (6) and (7). This is in general a nonlinear system that needs to be solved iteratively. The solution technique starts with an initial guess $\mathbf{x}(0)$ which is integrated forward in time using (2) to produce $\mathbf{x}(T)$. This initializes (via (7) ) the *backward* integration of the 'dual' or 'adjoint' dynamical equation

$$\frac{d\boldsymbol{\nu}}{dt} = -\boldsymbol{\nu}.\frac{\delta \mathbf{F}}{\delta \mathbf{x}} \qquad (8)$$

(with $\delta\mathbf{F}/\delta\mathbf{x}$ a matrix) from $t = T$ back to $t = 0$ to generate $\boldsymbol{\nu}(0)$. At this point, only two conditions remain to be satisfied. The Frechét derivative $\delta\mathcal{L}/\delta\mathbf{x}(0) := 2\lambda\mathbf{x}(0) - \boldsymbol{\nu}(0)$ will *not* in general vanish so the strategy is to move $\mathbf{x}(0)$ (subject to the initial distance constraint) until it does. By choosing to 'ascend' (moving $\mathbf{x}(0)$ in the direction of $\delta\mathcal{L}/\delta\mathbf{x}(0)$ ) a maximum in $\mathcal{L}$ is sought. The value of $\lambda$ is simultaneously specified by ensuring that $\|\mathbf{x}(0)\|_2 = d$ continues to hold during this adjustment in $\mathbf{x}(0)$. This procedure is repeated until $\|\delta\mathcal{L}/\delta\mathbf{x}(0)\|_2$ is sufficiently small to indicate a maximum. Theoretically, when $T \to \infty$, the global maximum

$$\max_{\mathbf{x}(0)} \mathcal{L} = \begin{cases} 0 & d < d_c, \\ \|\mathbf{X}_s - \mathbf{X}_0\|_2^2 & d = d_c, \\ \|\mathbf{X}_1 - \mathbf{X}_0\|_2^2 & d > d_c \end{cases} \qquad (9)$$

where $\mathbf{X}_1$ is another stable state of the system, $\mathbf{X}_s$ is a saddle embedded in the basin boundary with its only unstable manifold perpendicular to the boundary and in general $\|\mathbf{X}_s - \mathbf{X}_0\|_2 \neq \|\mathbf{X}_1 - \mathbf{X}_0\|_2$. This is just the statement that depending on whether the initial perturbation is strictly in the basin of attraction of $\mathbf{X}_0$, on the basin boundary or outside the basin (and in the basin of attraction of $\mathbf{X}_1$), the endstate is $\mathbf{X}_0$, $\mathbf{X}_s$ or $\mathbf{X}_1$ respectively for large times. The jump in the endstate distance is then discontinuous once $d$ reaches $d_c$ (a priori unknown) which signals that the basin boundary has been reached. The optimal disturbance $\mathbf{x}(0)$ at $d = d_c$ has been christened the 'minimal seed' [86, 87] since it is arbitrarily close to a disturbance which will trigger the transition from $\mathbf{X}_0$ to $\mathbf{X}_1$ for $d = d_c^+$. Put another way, the minimal seed, renormalised by a factor $1 + \epsilon$ where $\epsilon$ is vanishingly small but non-zero, represents the easiest/most efficient way to leave the basin of attraction of $\mathbf{X}_0$. Practically, this behaviour can be mimicked

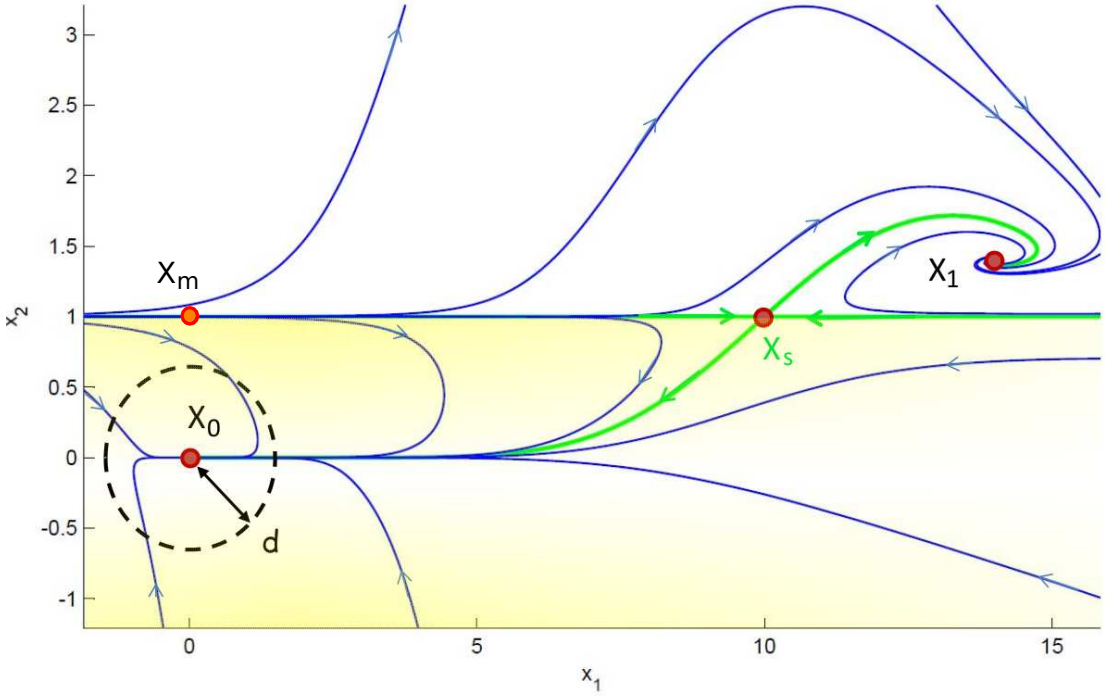


**Figure 1.** Phase portrait for the system defined by (10). The stable and unstable manifolds of $\mathbf{X}_s$ are drawn in thick green. A circle of radius $\|\mathbf{x}(0)\|_2 = d$ about $\mathbf{X}_0$ is shown as a dashed line. As the radius increases, the circle first touches the basin boundary at $\mathbf{X}_m = (0, 1)$ - the *minimal seed* since it is arbitrarily close to a state which will trigger the new asymptotic state $\mathbf{X}_1$ when the system is in state $\mathbf{X}_0$.

by choosing $T$ large enough that trajectories starting sufficiently close to the basin boundary but either side of it can be observed to diverge. The minimal seed is then approximated by the first initial condition as $d$ is increased which is observed to have escaped the basin of attraction of $\mathbf{X}_0$.

### *2.1. A simple example*

We show how this technique works for the simple two-dimensional system

$$\frac{d\mathbf{X}}{dt} = \begin{bmatrix} -X_1 + 10X_2 \\ X_2(10e^{-X_1^2/100} - X_2)(X_2 - 1) \end{bmatrix} \tag{10}$$

where $\mathbf{X} = (X_1, X_2)$ which has two local attractors at $\mathbf{X}_0 = (0, 0)$ and $\mathbf{X}_1 = (14.017, 1.4017)$. The basin boundary is simply $X_2 = 1$ which is the stable manifold of the saddle point at $\mathbf{X}_s = (10, 1)$: see Figure 1. All initial conditions with $X_2 < 1$ are attracted to $\mathbf{X}_0$, those with $X_2 > 1$ to $\mathbf{X}_1$, and those with $X_2 = 1$ to $\mathbf{X}_s$. Focussing on the 'unexcited' state $\mathbf{X}_0$, $\mathbf{x} := \mathbf{X} - \mathbf{X}_0$ and using the Euclidean norm again for simplicity, it is clear that drawing a circle in the $(x_1, x_2)$ plane centred on the origin and of increasing radius $d$, the basin boundary for $\mathbf{X}_0$ will be first touched at $d = d_c = 1$

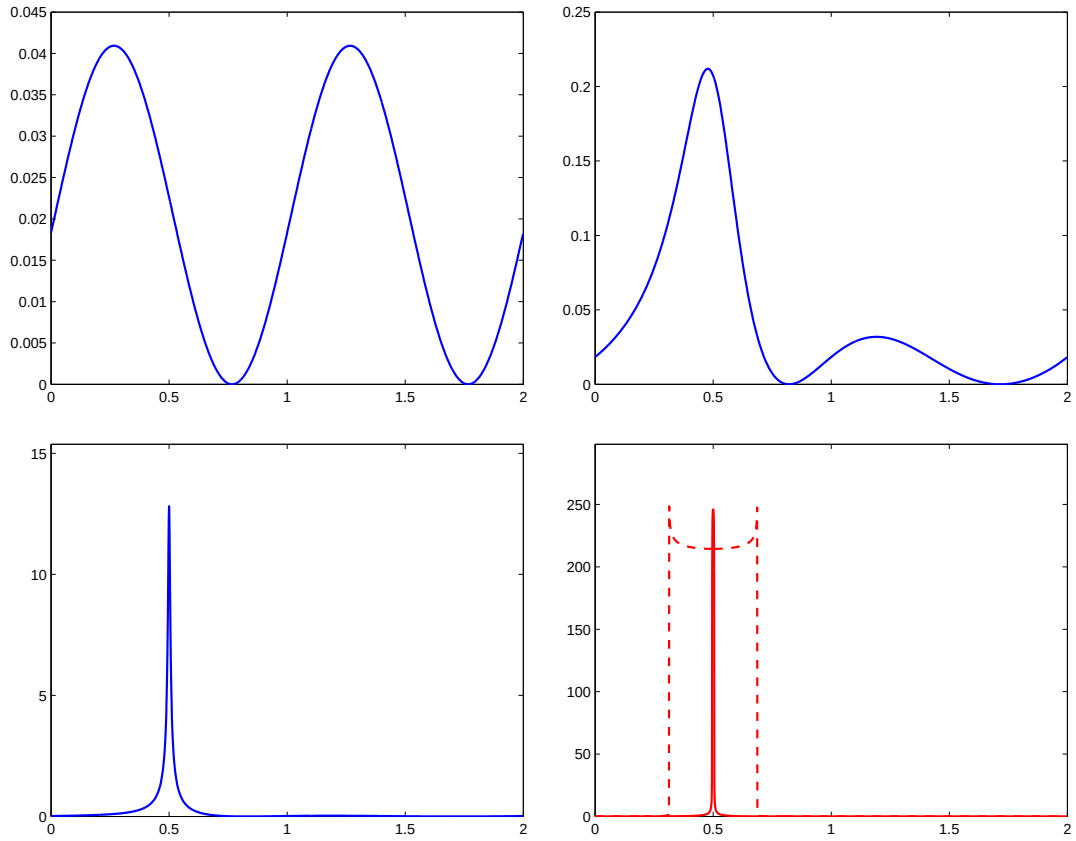


**Figure 2.** Top row: Gain $G := \|\mathbf{x}(t)\|_2^2/d^2$ verses $\theta$ for $T = 2$ and $d = 10^{-4}$ (top left) or 0.9 (top right). Bottom row: $\|\mathbf{x}(T)\|_2^2$ verses $\theta$ for $T = 2$ and $d = 0.9999$ (bottom left) or 1.0001 (solid line, bottom right) and 1.2 (dashed line, bottom right). Notice the sudden jump in $\|\mathbf{x}(T)\|_2^2$ when $d$ increases from 0.9999 to 1.0001 signalling that the basin boundary of $\mathbf{X}_0$ has been crossed ( $\|\mathbf{x}(T)\|_2^2$ is simply $100(1 - e^{-T})^2 + 1$ for $d = d_c$ ).

where $(x_1, x_2) = (0, 1)$: this is the *minimal seed* for this system. As $d$ increases beyond $d_c$, the basin boundary is increasingly punctured so that ever more initial conditions are outside of the basin of attraction of $\mathbf{X}_0$.

This observation can be deduced by iteratively solving the optimisation problem described above through integrating (10) forwards (since here $\mathbf{x} = \mathbf{X}$ as $\mathbf{X}_0 = \mathbf{0}$) to find $\mathbf{x}(t)$ and the dual dynamical equation

$$\frac{d\boldsymbol{\nu}}{dt} = \begin{bmatrix} \nu_1 + \frac{1}{5}x_1\nu_2(x_2^2 - x_2)e^{-x_1^2/100} \\ -10\nu_1 + \nu_2(3x_2^2 - 2x_2) - 10\nu_2(2x_2 - 1)e^{-x_1^2/100} \end{bmatrix} \tag{11}$$

for $\boldsymbol{\nu}(t)$ backwards (note that this backwards-in-time integration requires knowledge of $\mathbf{x}(t)$ across $[0, T]$). Figure 2 shows how $\|\mathbf{x}(T)\|_2^2$ varies over all permitted initial conditions parameterised by the angle $\theta \in [0, 2)$ where

$$\mathbf{x}(0) = ( d\cos\pi\theta, d\sin\pi\theta ) \tag{12}$$

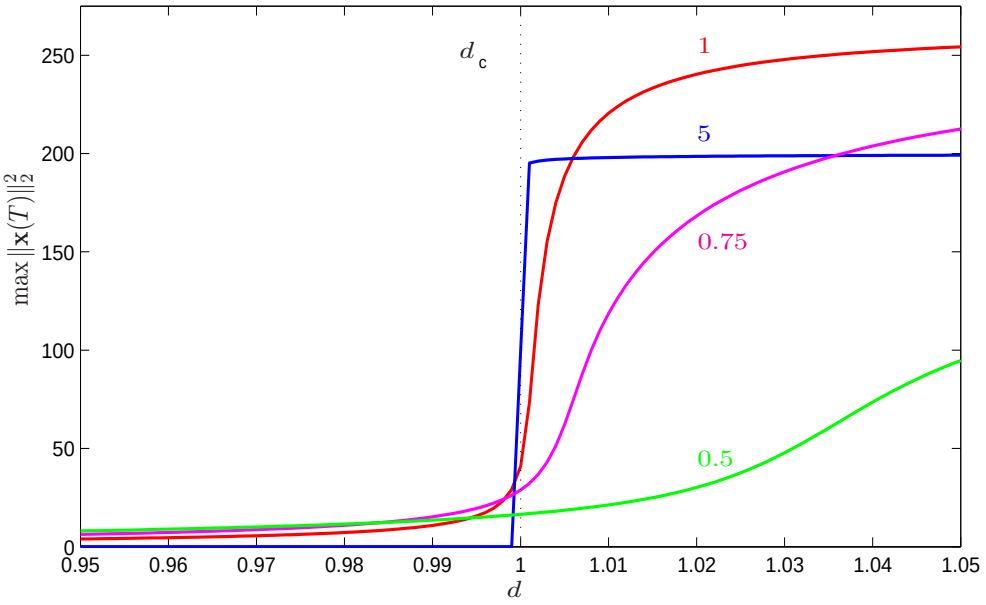


**Figure 3.** As $T$ (labelled on each curve) increases, the signature of the transition at $d_c$ becomes increasingly clear. Note only for $T \to \infty$ is the final plateau $\|\mathbf{x}(T)\|_2^2 = \|\mathbf{X}_1 - \mathbf{X}_0\|_2^2 \approx 198.5$ as $\mathbf{x}(t)$ 'overshoots': see Figure 1.

for selected values of $d$ and $T = 2$ (note the gain $G := \|\mathbf{x}(T)\|_2^2/d^2$ is plotted for the top row of subplots since $d$ has such different values). The small value $d = 10^{-4}$ is used to reproduce the linear result obtainable via standard matrix manipulations (see Appendix A) which possesses the $\mathbf{x}(0) \to -\mathbf{x}(0)$ ($\theta \to \theta \pm 1$) symmetry. As $d$ is increased, this symmetry is quickly destroyed as nonlinearity becomes important to indicate a unique optimal value of $\theta$ approaching 0.5 as $d \to d_c$. Once $d$ reaches $d_c$, $\|\mathbf{x}(T)\|_2^2$ jumps in value as the system explores the basin boundary and then (for $d > d_c$) the basin of attraction of $\mathbf{X}_1$. Three key points highlighted by this simple example are as follows.

(i) The importance of $T$ in determining $d_c$ to a required accuracy. Figure 3 shows that $d_c$ is increasingly well identified as the value of $T$ increases. Equivalently, if $T$ is too small, the jump in $\|\mathbf{x}(T)\|_2$ at $d = d_c$ is smeared out and so difficult to locate.

(ii) The minimal seed is *not* related to the linear optimal. For 'large' $T$ ($\geq 2$), the minimal seed has $\theta^* = 0.5$ ($90^o$) whereas the linear optimal ($d \to 0$) has $\theta^* \approx 0.2667$ ($48.0^o$). This is not surprising since phase space immediately around $\mathbf{X}_0$ is generally unrelated to the structure of the basin boundary a finite distance away. (The one caveat to this is if the nonlinear terms had been chosen to be energy-preserving - e.g. the model system studied in [27]. In this case, the dynamics are so tightly constrained in 2 dimensions that the minimal seed has to be the same as the linear optimal: see Appendix B for further discussion.)

(iii) The Euclidean norm works well as there is little growth for trajectories with $x_2 < 1$,

whereas trajectories in $x_2 > 1$ overshoot $\mathbf{X}_1$. If this were not the case, the functional to optimise - the objective functional - could be redesigned to signal the arrival in a new basin. Here for example, the value of $x_2(T)$ would be more appropriate with the Euclidean norm still used to constrain the competitor set of initial perturbations, i.e. the measure used as the objective functional and the norm constraining the initial condition do not need to be the same.

## 3. The Transition to Turbulence problem in Fluid Mechanics

We now move the discussion to fluid mechanics and a system described by a PDE. The breakdown of laminar shear flows has been a central problem in fluid mechanics since the inception of the subject and fascinated many generations of scientists (e.g. Rayleigh [91], Kelvin [105], Reynolds [95, 96], Orr [83], Sommerfeld [102], Noether [81], Taylor [103], Heisenberg [49], Landau [65], Hopf [51] and see the textbooks [17, 30, 29, 98]). Beyond a certain value of the driving rate (measured by a non-dimensional grouping called the Reynolds number $Re$ and generated by either imposed boundary motion, flow rate or pressure gradient), unidirectional shear flows (e.g. flow through a straight pipe) typically exhibit *bi*stability where a linearly-stable simple laminar state coexists with a spatially- and temporally-complicated turbulent state. The so-called 'transition' problem consists in understanding the physical processes by which ambient noise (present in any real flow) can trigger the observed transition of the flow from the laminar to the turbulent state. The fact that the laminar state is linearly stable means that the transition process is inherently nonlinear and even now still largely unexplained. The transition problem is not only a fascinating mathematical exercise in PDE theory, but the answers are crucial for informing attempts to inhibit (e.g. in the aircraft industry) or enhance (e.g. crucial for mixing processes) the phenonemon in practical applications.

In the last two decades or so, two complementary approaches to the transition problem have proved popular. The first - variously labelled 'transient growth', 'nonmodal stability theory' or 'optimal perturbation theory' - is a *linear* theory explaining how infinitesimal disturbances can experience large but transient magnification of their energy despite the laminar state being asymptotically stable (all the eigenvalues of the linearised evolution operator indicate exponential decay with time yet the operator is non-normal‡). This idea has a long history starting with Kelvin [105] and Orr [83] but has really only been systematically explored from the late 1980s onwards: see [12, 39, 48, 15, 108, 92], the reviews [46, 94, 97] and the books [98, 109]. The theory works well for interpreting finite time behaviour such as the flow response to noise immediately downstream of a pipe expansion [16] but actually says nothing about asymptotically long time behaviour. Initially, it was suggested that the presence of large transient growth could 'elevate' infinitesimal disturbances into the nonlinear regime where they could then become sustained (e.g.[4, 5]). While this

‡ An operator/matrix $L$ is non-normal if it does not commute with its adjoint/transpose $L^\dagger$ i.e. $LL^\dagger \neq L^\dagger L$.

picture, which emphasizes linear effects over nonlinearity, must be generally correct, no *quantitative* predictions of transition amplitudes can emerge without a fully nonlinear theory [111, 27].

The second approach to the transition problem, on the other hand, is fully nonlinear. This views the flow as a huge dynamical system and the flow state as an evolving trajectory in a phase space populated by various invariant sets (exact solutions) and their stable and unstable manifolds [34, 58, 35, 45, 26, 57]. From this perspective, 'transition' occurs when noise or a disturbance simply nudges the flow out of the basin of attraction of the laminar state. Making this observation more predictive has, however, been extremely hard due to the difficulty of mapping out the basin boundary. Some progress has been made shadowing the basin boundary (or the more general concept of an 'edge', which includes transient turbulence) *forward* in time using an 'edge tracking' technique [53, 101, 99]. This invariably leads to attracting regions of the basin boundary more distant (energetically) from the laminar state [87] and therefore less obviously relevant to the transition problem. What is really needed is a technique to track the basin boundary *backwards* in time to reach regions where it is close to the laminar state and so transition is most easily triggered.

The gap between these two approaches is therefore one of perspective: the optimal perturbation theory explains how infinitesimal disturbances can grow temporarily *within* the basin boundary whereas the dynamical systems approach focusses on what exists *beyond* the basin boundary. The new optimisation technique discussed in this article naturally bridges this gap by being able to examine how the linear optimal perturbation changes as the amplitude of the starting perturbation is increased until the basin boundary is reached. The original thinking behind the works [86, 87], however, was a little different being focussed on tracing the basin boundary or edge 'backwards' in time. Shadowing the basin boundary forwards using the edge tracking technique leads to relative attractors or 'edge states' on the basin boundary. This suggested an optimisation procedure to identify the closest point of approach of the basin boundary to the laminar state (the minimal seed). Assuming that this edge state is unique, then for all starting states *on* the basin boundary, the initial state which subsequently experiences the largest energy growth over asymptotically large times (so that all trajectories reach the edge state) *will* be the minimal seed [87]. While this optimisation problem itself is intractable because the basin boundary is unknown, it does suggest the tractable problem of finding the largest energy growth over all starting states of a given initial energy $E_0$. At precisely $E_0 = E_c$, where the basin boundary or edge touches the energy hypersurface at one velocity state, this optimization problem considers the growth of this state (the minimal seed) against the energy growth of all the other initial conditions below the edge. Given that these latter initial conditions lead to flows that grow initially but ultimately relax back to the basic state, the minimal seed will remain the optimal initial condition for the revised optimisation problem for large enough T [87]. The simple choice of the kinetic energy of the disturbance as both the objective functional *and* the constraining norm meant that the vanishing energy limit $E_0 \to 0$ lead back to

the familiar linear optimal perturbation calculation. It is now clear other choices could have been made for the objective functional providing it takes on heightened values for the turbulent state (e.g energy dissipation [73, 33]).

Before giving an example of the optimisation technique at work in fluid mechanics, we note that there has been many previous efforts to build upon (linear) optimal perturbation theory to design better ways to trigger transition. For example, by showing that the linear optimals can become unstable at sufficient amplitude (e.g. [114, 93]), or by designing a finite amplitude initial disturbance from a very small set of physically-motivated 'basis' states (e.g. [110, 32]), or by searching for optimal deformations of the *base flow* so as to create linear instability [13, 10, 44, 11].

### *3.1. The optimisation technique in pipe flow*

We now show the optimisation technique in action for the problem of incompressible fluid flow through a cylindrical pipe. This is a classical problem in fluid mechanics studied famously by Reynolds [95, 96] during which he first wrote down the non-dimensional grouping $Re$ now bearing his name. The flow can either be driven by imposing a constant pressure drop across the pipe or by imposing a constant mass flux through the pipe (e.g.[80]). We choose the former driving here as the formulation is slightly simpler (the latter is treated in [86, 87]): the two cases are equivalent for $L \to \infty$ and localised disturbances. The set up is an incompressible fluid of constant density $\rho$ and kinematic viscosity $\nu$ flowing in a circular pipe of radius $s_0$ under the action of a constant pressure drop across the pipe such that the applied pressure gradient is

$$\boldsymbol{\nabla} p^* = -\frac{4\rho\nu W}{s_0^2}\hat{\mathbf{z}}^* \tag{13}$$

and the Hagen-Poiseuille solution to the Navier-Stokes equations is

$$\mathbf{u}^*_{\text{lam}} := W\Big(1 - \frac{s^{*2}}{s_0^2}\Big)\hat{\mathbf{z}}^* \tag{14}$$

in the usual cylindrical coordinates $(s^*, \phi, z^*)$ aligned with the pipe axis. Non-dimensionalizing the system using the Hagen-Poiseuille centreline speed $W$ (e.g. $\mathbf{u}_{\text{lam}} := \mathbf{u}^*_{\text{lam}}/W$) and the pipe radius $s_0$ (so $s := s^*/s_0$) gives the Navier-Stokes equations

$$\frac{\partial \mathbf{u}_{\text{tot}}}{\partial t} + \mathbf{u}_{\text{tot}} \cdot \boldsymbol{\nabla}\mathbf{u}_{\text{tot}} + \boldsymbol{\nabla} p_{\text{tot}} - \frac{1}{Re}\nabla^2 \mathbf{u}_{\text{tot}} = \frac{4}{Re}\hat{\mathbf{z}} \tag{15}$$

(where $Re := s_0 W/\nu$ is the Reynolds number) to be solved subject to the boundary conditions

$$\mathbf{u}_{\text{tot}}(1, \phi, z, t) = \mathbf{0} \quad \& \quad \mathbf{u}_{\text{tot}}(s, \phi, z, t) = \mathbf{u}_{\text{tot}}(s, \phi, z + L, t). \tag{16}$$

The first is no-slip on the pipe wall at $s = 1$ and the second is periodicity over the (physical) length of $L$ radii along the pipe. We consider the energy growth (our 'distance' measure) of a finite-amplitude disturbance

$$\mathbf{u} := \mathbf{u}_{\text{tot}} - \mathbf{u}_{\text{lam}} \tag{17}$$

to the laminar profile $\mathbf{u}_{\rm lam} = (1-s^2)\hat{\mathbf{z}}$ by defining the Lagrangian

$$\begin{aligned}\mathcal{L} \quad &= \quad \mathcal{L}(\mathbf{u}, p, \lambda, \boldsymbol{\nu}, \pi; T, E_0) := \left\langle \frac{1}{2}|\mathbf{u}(\mathbf{x},T)|^2 \right\rangle + \lambda \left\{ \left\langle \frac{1}{2}|\mathbf{u}(\mathbf{x},0)|^2 \right\rangle - E_0 \right\} \\ &\quad + \int_0^T \left\langle \boldsymbol{\nu}(\mathbf{x},t) \cdot \left\{ \frac{\partial \mathbf{u}}{\partial t} + (\mathbf{u}_{\rm lam}\cdot\boldsymbol{\nabla})\mathbf{u} + (\mathbf{u}\cdot\boldsymbol{\nabla})\mathbf{u}_{\rm lam} + (\mathbf{u}\cdot\boldsymbol{\nabla})\mathbf{u} \right.\right. \\ &\quad \left.\left. + \boldsymbol{\nabla} p - \frac{1}{Re}\nabla^2\mathbf{u} \right\} \right\rangle dt + \int_0^T \langle \pi(\mathbf{x},t)\boldsymbol{\nabla}\cdot\mathbf{u}\rangle \, dt. \end{aligned} \tag{18}$$

where

$$\langle \ldots \rangle = \int_0^L \int_0^{2\pi} \int_0^1 \ldots s \mathrm{d}s \, \mathrm{d}\phi \, \mathrm{d}z \tag{19}$$

and $\lambda$, $\boldsymbol{\nu}$ and $\pi$ are Lagrangian multipliers imposing the constraints that the initial energy is fixed, that the Navier-Stokes equation holds over $t \in [0,T]$ and the flow is incompressible ( their corresponding Euler-Lagrange equations are respectively:

$$\left\langle \frac{1}{2}|\mathbf{u}(\mathbf{x},0)|^2 \right\rangle = E_0 \tag{20}$$

$$\frac{\partial \mathbf{u}}{\partial t} + (\mathbf{u}_{\rm lam}\cdot\boldsymbol{\nabla})\mathbf{u} + (\mathbf{u}\cdot\boldsymbol{\nabla})\mathbf{u}_{\rm lam} + (\mathbf{u}\cdot\boldsymbol{\nabla})\mathbf{u} + \boldsymbol{\nabla} p - \frac{1}{Re}\nabla^2\mathbf{u} = \mathbf{0}, \tag{21}$$

$$\boldsymbol{\nabla}\cdot\mathbf{u} = 0 \,). \tag{22}$$

The key additions to the well-known linear calculation acknowledging the fact that the disturbance is of finite amplitude are shown in red. The linearised problem is recovered in the limit of $E_0 \to 0$ whereupon the nonlinear term $\mathbf{u}\cdot\boldsymbol{\nabla}\mathbf{u}$ becomes vanishingly small relative to the other (linear) terms. On dropping this nonlinear term, the amplitude of the disturbance is then arbitrary for the purposes of the optimisation calculation and it is convenient to reset $E_0$ from vanishingly small to 1. The maximum of $\mathcal{L}$ is then precisely the maximum gain in energy over the period $[0,T]$.

The Euler-Lagrange equation for the pressure $p$ is

$$\begin{aligned} 0 &= \int_0^T \left\langle \frac{\delta \mathcal{L}}{\delta p}\delta p \right\rangle dt = \int_0^T \langle (\boldsymbol{\nu}\cdot\boldsymbol{\nabla})\delta p\rangle \, dt \\ &= \int_0^T \langle \boldsymbol{\nabla}\cdot(\boldsymbol{\nu}\delta p)\rangle \, dt - \int_0^T \langle \delta p(\boldsymbol{\nabla}\cdot\boldsymbol{\nu})\rangle \, dt. \end{aligned} \tag{23}$$

which vanishes if $\boldsymbol{\nu}$ satisfies natural boundary conditions (here, the same as those for $\mathbf{u}$) and

$$\boldsymbol{\nabla}\cdot\boldsymbol{\nu} = 0 \tag{24}$$

(note $\delta p$ is periodic across the pipe to ensure the pressure drop across the pipe is constant). The variation in $\mathcal{L}$ due to $\mathbf{u}$ (with $\delta\mathbf{u}$ satisfying (16) ) is

$$\delta\mathcal{L} = \int_0^T \left\langle \frac{\delta\mathcal{L}}{\delta\mathbf{u}}\cdot\delta\mathbf{u} \right\rangle = \langle \mathbf{u}(\mathbf{x},T)\cdot\delta\mathbf{u}(\mathbf{x},T)\rangle + \lambda \langle \mathbf{u}(\mathbf{x},0)\cdot\delta\mathbf{u}(\mathbf{x},0)\rangle \tag{25}$$

$$+ \int_0^T \left\langle \boldsymbol{\nu}\cdot\left\{ \frac{\partial\delta\mathbf{u}}{\partial t} + (\mathbf{u}_{\rm lam}\cdot\boldsymbol{\nabla})\delta\mathbf{u} + (\delta\mathbf{u}\cdot\boldsymbol{\nabla})\mathbf{u}_{\rm lam} \right.\right. \tag{26}$$

$$+\mathbf{u}.\boldsymbol{\nabla}\delta\mathbf{u} + \delta\mathbf{u}\cdot\boldsymbol{\nabla}\mathbf{u} - \frac{1}{Re}\nabla^2\delta\mathbf{u}\Big\}\Big\rangle\, dt + \int_0^T \langle\pi\boldsymbol{\nabla}\cdot\delta\mathbf{u}\rangle\, dt. \tag{27}$$

The first term in the second line of the above equation can be reexpressed as

$$\begin{aligned}\int_0^T \left\langle \boldsymbol{\nu}\cdot\frac{\partial\delta\mathbf{u}}{\partial t}\right\rangle dt &= \int_0^T \left\langle \frac{\partial}{\partial t}(\delta\mathbf{u}\cdot\boldsymbol{\nu})\right\rangle dt - \int_0^T \left\langle \delta\mathbf{u}\cdot\frac{\partial\boldsymbol{\nu}}{\partial t}\right\rangle dt \\ &= \langle\delta\mathbf{u}(\mathbf{x},T)\cdot\boldsymbol{\nu}(\mathbf{x},T) - \delta\mathbf{u}(\mathbf{x},0)\cdot\boldsymbol{\nu}(\mathbf{x},0)\rangle - \int_0^T \left\langle \delta\mathbf{u}\cdot\frac{\partial\boldsymbol{\nu}}{\partial t}\right\rangle dt, \end{aligned}\tag{28}$$

the second term as

$$\begin{aligned}\langle\boldsymbol{\nu}\cdot\{(\mathbf{u}_{\text{lam}}\cdot\boldsymbol{\nabla})\delta\mathbf{u}\}\rangle &= \langle\boldsymbol{\nabla}\cdot((\boldsymbol{\nu}\cdot\delta\mathbf{u})\mathbf{u}_{\text{lam}}) - \delta\mathbf{u}\cdot\{(\mathbf{u}_{\text{lam}}\cdot\boldsymbol{\nabla})\boldsymbol{\nu}\}\rangle \\ &= -\langle\delta\mathbf{u}\cdot\{(\mathbf{u}_{\text{lam}}\cdot\boldsymbol{\nabla})\boldsymbol{\nu}\}\rangle, \end{aligned}\tag{29}$$

the third term as

$$\langle\boldsymbol{\nu}\cdot\{(\delta\mathbf{u}\cdot\boldsymbol{\nabla})\mathbf{u}_{\text{lam}}\}\rangle = \left\langle\delta\mathbf{u}\cdot\left\{\boldsymbol{\nu}\cdot(\boldsymbol{\nabla}\mathbf{u}_{\text{lam}})^{\mathrm{T}}\right\}\right\rangle \quad (=\langle\delta u_i\ \nu_j\ \partial_i u_{\text{lam},j}\rangle). \tag{30}$$

the fourth and fifth as

$$\langle\boldsymbol{\nu}\cdot(\delta\mathbf{u}\cdot\boldsymbol{\nabla}\mathbf{u} + \mathbf{u}\cdot\boldsymbol{\nabla}\delta\mathbf{u})\rangle = \left\langle\delta\mathbf{u}\cdot\left([\boldsymbol{\nabla}\mathbf{u}]^T\cdot\boldsymbol{\nu} - \mathbf{u}\cdot\boldsymbol{\nabla}\boldsymbol{\nu}\right)\right\rangle \tag{31}$$

and the sixth term as

$$\left\langle\boldsymbol{\nu}\cdot\left(-\frac{1}{Re}\nabla^2\delta\mathbf{u}\right)\right\rangle = -\left\langle\frac{1}{Re}\delta\mathbf{u}\cdot\nabla^2\boldsymbol{\nu}\right\rangle, \tag{32}$$

and finally the last term as

$$\begin{aligned}\langle\pi\boldsymbol{\nabla}\cdot\delta\mathbf{u}\rangle &= \langle\boldsymbol{\nabla}\cdot\pi\delta\mathbf{u}\rangle - \langle\delta\mathbf{u}\cdot\boldsymbol{\nabla}\pi\rangle \\ &= -\langle\delta\mathbf{u}\cdot\nabla\pi\rangle. \end{aligned}\tag{33}$$

where $\pi$ has to be periodic as $\langle\delta\mathbf{u}\cdot\hat{\mathbf{z}}\rangle \neq 0$ (a change in the mass flux is permitted for constant pressure-drop driven flow) for the surface term to drop. Combining all these gives

$$\begin{aligned}\int_0^T \left\langle\frac{\delta\mathcal{L}}{\delta\mathbf{u}}\cdot\delta\mathbf{u}\right\rangle &= \langle\delta\mathbf{u}(\mathbf{x},T)\cdot\{\mathbf{u}(\mathbf{x},T) + \boldsymbol{\nu}(\mathbf{x},T)\}\rangle \\ &\quad + \langle\delta\mathbf{u}(\mathbf{x},0)\cdot\{\lambda\mathbf{u}(\mathbf{x},0) - \boldsymbol{\nu}(\mathbf{x},0)\}\rangle \\ &\quad + \int_0^T \left\langle\delta\mathbf{u}\cdot\left\{-\frac{\partial\boldsymbol{\nu}}{\partial t} - ([\mathbf{u}_{\text{lam}}+\mathbf{u}]\cdot\boldsymbol{\nabla})\boldsymbol{\nu} + \boldsymbol{\nu}\cdot(\boldsymbol{\nabla}[\mathbf{u}_{\text{lam}}+\mathbf{u}])^{\mathrm{T}}\right.\right. \\ &\qquad \left.\left. -\boldsymbol{\nabla}\pi - \frac{1}{Re}\nabla^2\boldsymbol{\nu}\right\}\right\rangle dt. \end{aligned}\tag{34}$$

For this to vanish for all allowed $\delta\mathbf{u}(\mathbf{x},T)$, $\delta\mathbf{u}(\mathbf{x},0)$ and $\delta\mathbf{u}(x,t)$ with $t\in(0,T)$ means

$$\frac{\delta\mathcal{L}}{\delta\mathbf{u}(\mathbf{x},T)} = \mathbf{0} \quad\Rightarrow\quad \mathbf{u}(\mathbf{x},T) + \boldsymbol{\nu}(\mathbf{x},T) = \mathbf{0}, \tag{35}$$

$$\frac{\delta\mathcal{L}}{\delta\mathbf{u}(\mathbf{x},0)} = \mathbf{0} \quad\Rightarrow\quad \lambda\mathbf{u}(\mathbf{x},0) - \boldsymbol{\nu}(\mathbf{x},0) = \mathbf{0}, \tag{36}$$

$$\frac{\delta\mathcal{L}}{\delta\mathbf{u}} = \mathbf{0} \quad\Rightarrow\quad \frac{\partial\boldsymbol{\nu}}{\partial t} + (\mathbf{u}_{\text{lam}}+\mathbf{u})\cdot\boldsymbol{\nabla}\boldsymbol{\nu} - \boldsymbol{\nu}\cdot(\boldsymbol{\nabla}[\mathbf{u}_{\text{lam}}+\mathbf{u}])^{\mathrm{T}} + \boldsymbol{\nabla}\pi + \frac{1}{Re}\nabla^2\boldsymbol{\nu} = \mathbf{0}. \tag{37}$$

This last equation is the *dual* (or adjoint) Navier-Stokes equation for evolving $\boldsymbol{\nu}$ *backwards* in time because of the negative diffusion term. This dual equation has the same means of driving - constant pressure drop - as the physical problem, a situation also true for the constant mass-flux situation [86, 87]

The approach for tackling this optimization problem is iterative as in the linear situation [68, 2, 24, 69, 47] (see also the review [70]), the nonlinear calculation of [116] using the (parabolic) boundary layer equations and is essentially as outlined in §2.

**Step.0** Choose an initial condition $\mathbf{u}^{(0)}(\mathbf{x},0)$ such that

$$\left\langle \frac{1}{2}|\mathbf{u}^{(0)}(\mathbf{x},0)|^2 \right\rangle = E_0. \tag{38}$$

The (better) next iterate $\mathbf{u}^{(n+1)}(\mathbf{x},0)$ is then constructed from $\mathbf{u}^{(n)}(\mathbf{x},0)$ as follows:

**Step 1.** Time integrate the Navier-Stokes equation (21) forward with incompressibility $\nabla\cdot\mathbf{u}=0$ and using the boundary conditions (16) from $t=0$ to $t=T$ with the initial condition $\mathbf{u}^{(n)}(\mathbf{x},0)$ to find $\mathbf{u}^{(n)}(\mathbf{x},T)$.

**Step 2.** Calculate $\boldsymbol{\nu}^{(n)}(\mathbf{x},T)$ using (35) which is then used as the *initial* condition for the dual Navier-Stokes equation (37).

**Step 3.** Backwards time integrate the dual Navier-Stokes equation (37) with incompressibility (24) and boundary conditions (16) from $t=T$ to $t=0$ with the 'initial' condition $\boldsymbol{\nu}^{(n)}(\mathbf{x},T)$ to find $\boldsymbol{\nu}^{(n)}(\mathbf{x},0)$.

**Step 4.** Use the fact that

$$\frac{\delta\mathcal{L}}{\delta\mathbf{u}(\mathbf{x},0)} = \lambda\mathbf{u}(\mathbf{x},0) - \boldsymbol{\nu}(\mathbf{x},0) \tag{39}$$

is now computable to move $\boldsymbol{\nu}(\mathbf{x},0)$ towards a maximum of $\mathcal{L}$. One approach [86, 87, 89] is to simply move $\mathbf{u}^{(n)}(\mathbf{x},0)$ in the direction of maximum ascent of $\mathcal{L}$, i.e. a correction to $\mathbf{u}^{(n)}$ is calculated as follows:

$$\mathbf{u}^{(n+1)} = \mathbf{u}^{(n)} + \epsilon\left[\frac{\delta\mathcal{L}}{\delta\mathbf{u}(\mathbf{x},0)}\right]^{(n)} \tag{40}$$

$$= \mathbf{u}^{(n)} + \epsilon\left(\lambda\mathbf{u}^{(n)}(\mathbf{x},0) - \boldsymbol{\nu}^{(n)}(\mathbf{x},0)\right), \tag{41}$$

with $\lambda$ chosen such that

$$E_0 = \left\langle \frac{1}{2}|\mathbf{u}^{(n+1)}(\mathbf{x},0)|^2 \right\rangle \tag{42}$$

$$= \left\langle \frac{1}{2}|(1+\epsilon\lambda)\mathbf{u}^{(n)}(\mathbf{x},0) - \epsilon\boldsymbol{\nu}^{(n)}(\mathbf{x},0)|^2 \right\rangle. \tag{43}$$

Here $\epsilon$ is a parameter which can be adjusted as the iteration proceeds to improve convergence (e.g. [87, 89]).

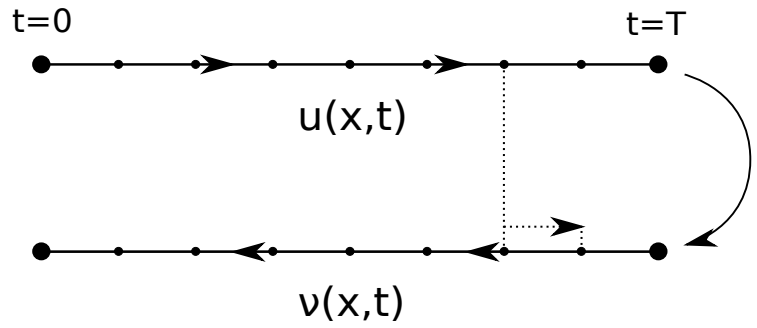


**Figure 4.** Checkpointing: during the (backward-in-time) calculation of $\boldsymbol{\nu}(\mathbf{x},t)$ the velocity $\mathbf{u}(\mathbf{x},t)$ is recalculated in short sections from each checkpoint (shown as dots on the forward-in-time calculation.

Other strategies have been adopted - e.g. a relaxation approach [73, 33] or a conjugate gradient method [18, 19, 20, 21] - but it is presently unclear which, if any, is superior ([86] also experimented with the conjugate gradient method but found no noticeable improvement in convergence).

The iterations are repeated until some convergence criterion is fulfilled. Some authors [86, 87, 89] have concentrated on how the residual $\langle(\delta\mathcal{L}/\delta\mathbf{u}(\mathbf{x},0))^2\rangle$ behaves as a function of the iteration number and others [18, 19, 20, 21] have focussed on the incremental change in $\mathcal{L}$ between iterations. The former seems more natural given the latter depends on how large a step is taken in moving $\mathbf{u}(\mathbf{x},0)$ but has its issues too (e.g. figure 9 in [87], figure 9(b) in [89]). More work is needed to identify a robust convergence criterion.

There is one further practical issue which needs to be discussed when the fully nonlinear optimisation problem is considered: the dual Navier-Stokes equation is linear in $\boldsymbol{\nu}$ but depends on $\mathbf{u}(\mathbf{x},t)$. This field either needs to be stored in totality (over the whole volume and time period), which is only practical for low resolution, short integrations, or must be recalculated piecemeal during the backward integration stage. This latter 'check-pointing' approach [8, 50] requires that $\mathbf{u}$ is stored at regular intermediate points, e.g. $t = T_i := iT_{opt}/n$ for $i = 1, \ldots, n-1$, during the forward integration stage. Then to integrate the adjoint equation backward over the time interval $[T_i, T_{i+1}]$, $\mathbf{u}$ is regenerated starting from the stored value at $t = T_i$ by integrating the Navier-Stokes equations forward to $T_{i+1}$ again: see Figure 4. The extent of the check pointing is chosen such that the storage requirement for each subinterval is manageable. The extra overhead of this technique is to redo the forward integration for every backward integration, so approximately a 50% increase in cpu time, assuming forward and backward integrations take essentially the same time. As memory restrictions may make full storage impossible, this is a small price to pay.

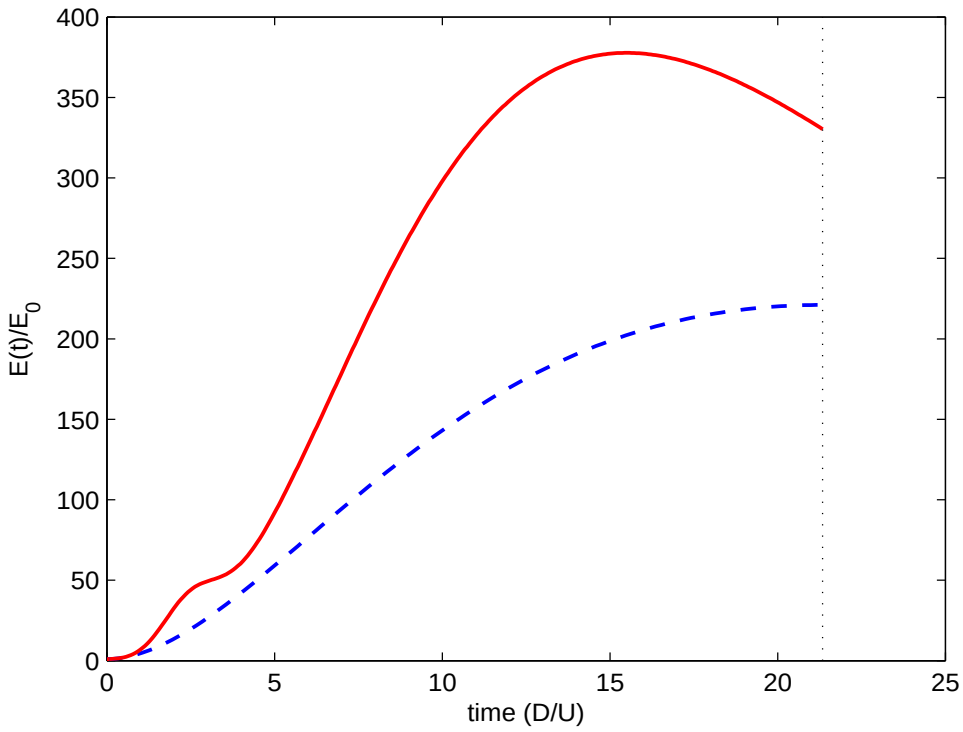


**Figure 5.** Pipe flow: the evolution of the linear and nonlinear energy growth optimals at $Re = 1750$ in a pipe of length $\pi$ radii and constant flux [86]. The blue dashed line corresponds to the linear optimal for $E_0 \to 0$ whereas the red solid line is the nonlinear optimal for $\approx 1.5E_{3d}$ both calculated using (a short) $T$ equal to the linear growth optimal time shown as a vertical black dotted line (the nonlinear optimal actually produces even more growth at a slightly earlier time).

### *3.2. Results: Minimal seeds and routes to turbulence*

In fluid mechanics, the kinetic energy of the perturbation $\mathbf{u}$ (defined in (17)) has invariably been used as the norm to constrain the competitor initial conditions in the optimisation problem and typically also used as the objective functional to be optimised. However a different objective functional can be chosen provided it clearly takes on larger values in the turbulent state than those reached in the basin of attraction of the laminar state (e.g. viscous dissipation rate or even the total viscous dissipation over the period $[0, T]$ - [73, 33]).

After these choices, the optimisation problem has two operational inputs - the time horizon $T$ and the initial 'distance' $d$ (read energy $E_0$ for the rest of this section) - beyond a complete specification of the system parameters (e.g. $Re$ and length of pipe in pipe flow).

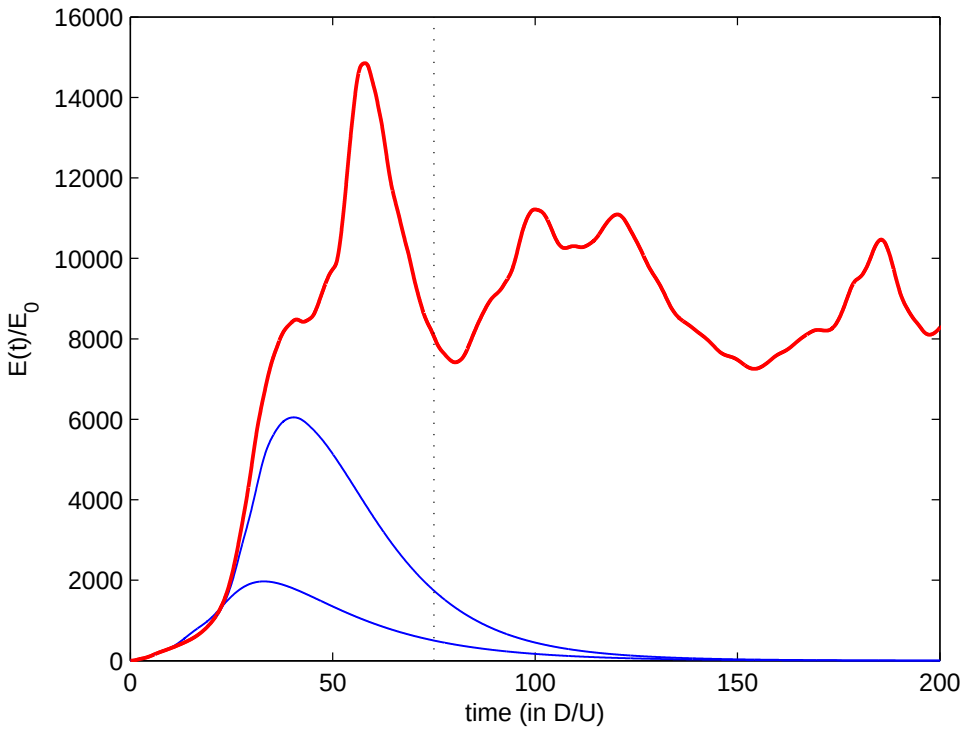


**Figure 6.** Pipe flow: the evolution of the energy growth optimals at $Re = 2400$ in a constant-flux pipe of length 10 radii using a 'large' time $T = 75\,D/U$ indicated by a vertical black dotted line (see section 5 of [87]). The thin blue lines correspond to the NLOPs for two $E_0$s just below $E_c$ (within 1%) with turbulence not triggered. The thick red solid line is for $E_0$ just above $E_c$ (again within 1%) and turbulence is now clearly triggered (see figure 7 for snapshots of this evolution).

*3.2.1. Large $T$* The approach for identifying the minimal seed outlined above is to choose a large fixed value of $T$ and to explore how the global optimal value behaves as $E_0$ is increased from zero [86, 87, 89] (complementary work [73, 33] instead reduces $E_0$ until no turbulent state is found). This was first pursued for the full Navier-Stokes equations in pipe flow [86] where the *l*inear ($E_0 \to 0$) energy growth *o*ptimal *p*erturbation - hereafter referred to as the 'LOP' - is 2-dimensional (streamwise-independent). The optimal for small but finite $E_0$ is a smooth nonlinear adjustment of the linear result retaining its 2 dimensionality and with a slightly reduced energy gain. Beyond an initial critical energy $E_{3d}$, however, a new completely different 3-dimensional perturbation was found as the global optimal and christened the 'NLOP' (*n*on*l*inear *o*ptimal *p*erturbation) [86]: see Figure 5. This NLOP reflects a clear strategy by the fluid to spatially localise the starting perturbation so that its peak amplitude is larger but only over a limited volume to cheat the global energy constraint. The original pipe geometry used in [86] was very short so the NLOP is only localised in

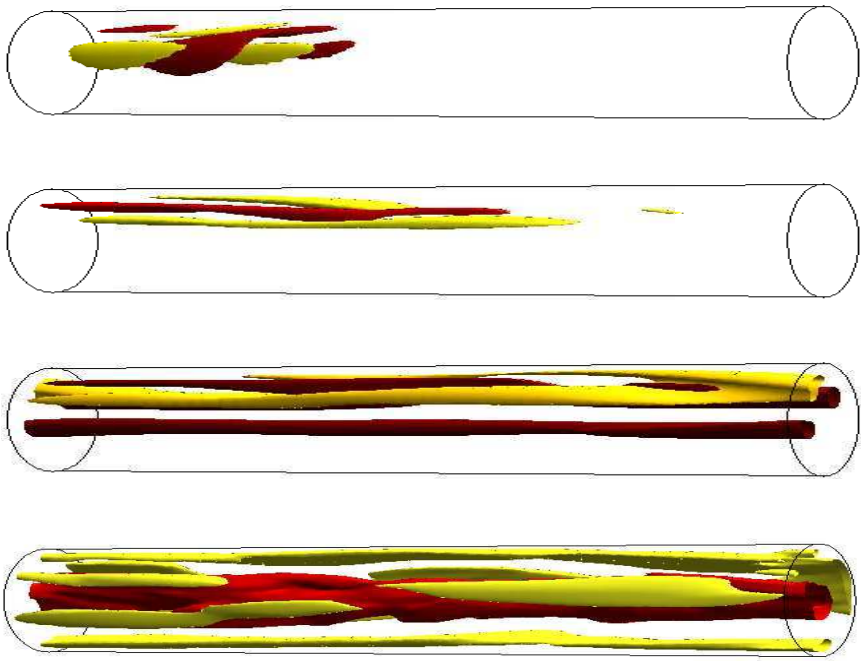

**Figure 7.** Pipe flow: snapshots showing the evolution (time running downwards and fluid flow left to right) of a turbulence-triggering perturbation which approximates the minimal seed in a 10 radii long pipe at $Re = 2400$ (constant flux) [87] (the corresponding evolution of the total energy is shown as the red thick line in figure 6). The isocontours in each plot correspond to 50% of the maximum (light/yellow) and 50% of the minimum (dark/red) of the streamwise perturbation velocity in the pipe at $t = 0$ (top: essentially the minimal seed), $t = 5$ (second down), $t = 20$ (third down) and $t = 75\,D/U$ (bottom: the target time). The perturbation energy is initially localised but quickly spreads out to generate streamwise streaks (by $t \approx 10$) which then break up to generate turbulence.

the radial and azimuthal directions (see Figure 2(a) in [86]). Subsequent computations in much longer pipe geometries have confirmed that the NLOP fully localises by also localising in the axial (streamwise) direction too [87, 88]: see Figure 7. Physically, the NLOP evolves by initially 'unpacking' (delocalising) under the influence of the background shear flow and taking advantage of 3 distinct linear mechanisms for transient growth: the Orr mechanism which occurs quickly, oblique wave growth which operates over an intermediate timescale, and lift-up which occurs over a slow timescale. These mechanisms are unrelated in the linear problem i.e. initial conditions exploiting each are distinct from each other so that the mechanisms do not combine. However they can communicate with the addition of nonlinearity which allows each mechanism to 'pump prime' the next generating a much higher overall growth [87, 33]. Figure 5 shows a period of growth in the NLOP curve (the oblique wave growth stage) which terminates at $t \approx 2.5$ before further growth (lift up) occurs until $t \approx 16$ (the Orr mechanism occurs

over a much faster timescale - $O(0.1)$ see Figure 1 of [87] - and is therefore hidden in this plot). Appendix B discusses a very simple model to illustrate this phenomenon (compare Figures 5 and 9).

As $E_0$ is increased further, this NLOP remains the global optimal until another critical energy $E_{fail}$ is reached beyond which the optimisation procedure fails to converge. Pringle et al. [87] interpret (their conjecture 1) that this corresponds to the first energy at which an initial condition can reach the turbulent state since then the extreme sensitivity of the final-state energy at $T$ to changes in the initial condition, due to exponential divergence of adjacent states will effectively mean non-smoothness and prevent convergence. That the turbulent state has been reached at $E_{fail}$ is easily confirmed by examining the endstates $\mathbf{u}(\mathbf{x}, T)$ reached as part of the iteration algorithm so that $E_{fail}$ is at least an upper bound on the true critical energy $E_c$, which is the lowest energy at which turbulence can be triggered. Arguing that in fact $E_{fail} = E_c$ requires a belief or hope that the search algorithm will find any state on the (initial) energy hypersurface which can reach the turbulent state if it exists. This is never likely to be proved but can at least be made plausible by rerunning the algorithm with a variety of initial starting states (e.g. see Figure 14 in [87]).

Pringle et al. [87] also noticed (their conjecture 2) that the NLOP converged to the minimal seed as $E_0 \to E_c^-$ for their choice of the energy functional. It now seems clear that there is nothing special about using the perturbation energy as an objective functional merely that it is one of a class of functionals which take on heightened values for turbulent flows. Providing such a functional is chosen, the best way to maximise it should be to get as close to the basin boundary as possible while remaining on the $E_0$ hypersurface since all other states will be sucked into the laminar state if $T$ is chosen larger than the typical transient growth time. This is certainly borne out by comparing estimates for $E_c$ and the corresponding minimal seed found in plane Couette flow using the total viscous dissipation over $[0, T]$ [73] or the final energy growth [89] as objective functionals. One of the motivations for choosing the total dissipation over the time period in [73, 33] was to capture the fastest transition. Finding the critical energy, however, is a problem in finding just one state which triggers turbulence so, conceptually, the final viscous dissipation rate could have been used just as well (although practically, time averaging the dissipation rate helped smoothen the effect of dealing with turbulent endstates in their optimisation algorithm).

*3.2.2. Optimising over $T$* Given the need to choose $T$ 'large enough', one natural idea has been to 'optimise it out of the problem' by asking the question 'for a given initial perturbation of energy $E_0$ what is the largest growth over *any* $T$?' Algorithmically, this requires only a small change but can dramatically alter the results for $E_0 < E_c$. Work by [89] in plane Couette flow has shown how a LOP achieving large growth at small times can 'mask' the emergence of a NLOP (which has a longer growth time) as $E_0$ increases (see their Figure 2). When $E_c$ is reached, however, there is the same leap in optimal value which is now also accompanied with a sudden leap in the optimal time

$T$ (e.g. see Figures 3 and 10 in [89]). Operationally, this means that the minimal seed (and $E_c$) can still be found albeit only when the algorithm fails to converge rather than as a smooth convergence procedure for as $E_0$ approaches $E_c$ from below.

*3.2.3. Small $T$* Cherubini and coworkers [18, 19, 20] have computed the nonlinear optimal energy growth disturbances for small $T$ in boundary layer flow. This is a particularly challenging system since the flow is spatially developing and open (flow leaving the computational domain is not recycled using periodic boundary conditions) making longer time runs very expensive. Rather than isolating minimal seeds§, their focus has been to establish that nonlinear mechanisms can enhance transition by uncovering energies $E_0$ where the NLOP subsequently triggers turbulence (when integrated beyond $T$) whereas the linear optimal, scaled up in energy, does not. By analysing the transition path of their NLOP in detail, they find a number of mechanisms believed generic to boundary layer transition [19, 20]. Some of these appear to carry over to plane Couette flow [21] when transition is studied again using short-time optimisation analysis. Here, for small $T$, at least two scenarios are found: a 'highly dissipative' bursting path and short-path depending on how close the perturbation is initially to the basin boundary.

### *3.3. Summary*

The key points to note in applying this variational approach in fluid mechanics are as follows.

(i) The choice of objective functional is not important provided it takes on heightened values for turbulent flows compared to the laminar state. The algorithm works best when there is a good separation between functional values attained within the basin of attraction and the turbulent state. This is typically the case for final time values of the perturbation kinetic energy or viscous dissipation rate when the flow domain is large enough, and $Re$ is not too close to the critical value at which the turbulent state first appears [87].

(ii) When seeking the transition threshold $E_c$, $T$ needs to be large enough to avoid two problems: a) possible transients with large growth caused by some parts of the basin boundary attaining large functional values, and b) to allow sufficient times for states to reach the turbulent attractor [87, 89].

(iii) The minimal seed can either be identified smoothly as a converged NLOP for $E_0 \to E_c^-$ at fixed but large $T$ [87] or as the first initial condition encountered by the algorithm which triggers turbulence as $E_0$ is increased if $T$ is being optimised over [89].

§ Note Cherubini and coworkers [18, 19, 20] use the term 'minimal seed' differently to this article: they use it to describe the minimal spatial structure found in their NLOPs whereas here it is the minimal energy state, when infinitesimally disturbed, to trigger turbulence.

Finally, we end this section with a note of caution. The approach relies on the correct identification of the global optimal to a (non-convex) nonlinear optimisation problem. There is unlikely to ever been a formal criterion to verify that this has been accomplished (in contrast to the linearised problem) so care must be taken to collect supporting evidence for this claim if possible. So far, the results obtained have been checked for consistency in a number of different ways:

(i) Robustness: it is clearly good practice to check global optimality by seeding the variational algorithm with a suite of very different initial states to see if the same optimal emerges each time (e.g. Figures 14 and 15 of [87]) or, if not, that the new optimal is just a local optimal.

(ii) Physical plausibility: it is reassuring that the NLOPs found are localised and appear to 'join up' the various hitherto-unconnected linear energy-growth mechanisms during their evolution [87, 19, 33].

(iii) Using different objective functionals: the cross-checking of results between two groups [73, 89] using different algorithms and objective functionals has been crucial in establishing the feasibility of this approach to realistics problems in fluid mechanics.

(iv) Of all the states on the basin boundary, the minimal seed should experience the largest increase in 'distance' (read perturbation energy) as it evolves up to the edge state and states 'close' to the minimal seed should evolve to pass close to the edge state before either relaminarising or trigger turbulence (e.g. Figure 17 of [87]).

## 4. Applications

### *4.1. Climate modelling and Weather Forecasting*

In climate modelling and weather forecasting, the sensitivity of predictive models to uncertainty in their initial conditions (the current best guess of the model's state) is of central importance. Lorenz [67] was the first to introduce the concept of singular vectors as a way to analyse how this uncertainty (presumed small) may grow with time. However, it wasn't until the late 1980s when the idea really took hold following the work of Farrell [40, 41] in atmospherics and the accompanying realisation in general shear flows of the phenomenon of (linear) transient growth or (linear) 'optimal perturbations' [12, 39, 48, 15, 108, 92]. This quickly led to the implementation of singular vectors to generate ensemble forecasts (e.g. at the European Centre for Medium-Range forecasting (ECMWF) [84, 14]).

The initial uncertainties, however, needn't be small and their true behaviour with time may differ significantly from that given by the evolution operator linearised around the base solution. As a result, there have been attempts to include some nonlinearity into the problem by an iterative approach [82, 6] as well as a proposal for a fully nonlinear approach by Mu and coworkers: [74, 75, 77, 78, 79] and more recently [31, 115, 55]. [75] in particular introduced the concept of a 'Conditional nonlinear optimal perturbation'

(CNOP), which is exactly the NLOP discussed above, to study the predictability of a very simple coupled atmosphere-ocean model. As mentioned in the Introduction, the idea to study the transitions between different stable states was also suggested by Mu and co-workers in the context of ocean modelling where multiple equilibria are a generic feature of general circulation models. To illustrate this idea, [76] studied a very simple box model of the thermohaline circulation consisting of 2 ODEs using CNOPs. Subsequent work has tried to scale up the calculation of CNOPs to realistic PDE models with [77] computing CNOPs for a 2D quasigeostrophic model with 512 grid points and [104] treating a 2D barotropic double-gyre ocean flow model with 4800 degrees of freedom. The latter study, however, concluded that finding basin boundaries was just too computationally expensive to attempt. Given the recent successes in the transition problem, this conclusion probably deserves to be revisited.

Before leaving this section, the work of Toth and Kalnay [106, 107, 56] on the so called 'breeding' method deserves mention. This consists of adding a small arbitrary perturbation to the full forecasting model, allowing this to evolve and then rescaling it after a given time to reseed the next forecast period. This procedure, which breeds 'bred vectors', is less optimal in identifying optimal perturbations for a given period (in fact perturbations which emerge have *just* grown the fastest rather than *will* grow the fastest) but is readily generalised to incorporate the finite-amplitude nature of the uncertainties since the full forecasting model is used. This method is used to generate ensemble forecasts at the National Centers for Environmental Prediction (NCEP) (formerly the US National Meteorological Center).

### *4.2. Thermoacoustics*

The idea of using an optimisation approach to locate a basin boundary was also introduced to the field of thermoacoustics at the same time as in the transition to turbulence community. [62] treated a simple model of thermoacoustic system - a horizontal Rijke tube - and showed that a sufficiently large impulse can trigger a self-sustained oscillation using the strategy discussed in this article. This model system is sufficiently simple (a couple of time-dependent 1-space dimension PDEs) to perform an exhaustive survey of transient growth possibilities over amplitude and event horizon $T$ [63] as well as including noise [112]. It is also realistic enough to achieve some correspondence with experiments [54].

### *4.3. Control*

Work in controlling fluid flows has long flirted with fully nonlinear methods (e.g. [9]) but they remain currently very expensive and probably still impractical [60]. The recent success in calculating identifying NLOPs and minimal seeds, however, has lead to some new activity in this direction. [85] has recently used the adjoint-based optimisation procedure discussed here for the full Navier-Stokes equations to control the 2D boundary layer dynamics over a bump by blowing and sucking appropriately

through the boundaries. This work has been subsequently extending to 3D [22] where initial conditions corresponding to the LOP and NLOP have been treated.

In a slightly different vein, a more *nonlinearly stable* plane Couette flow has been designed by imposing spanwise oscillations on the usual streamwise boundary shearing [90]. This work builds upon the fact that if the critical energy of the minimal seed can be found then new boundary conditions can be designed to increase this energy thereby improving the stability of the base state. While the choice of imposing spanwise oscillations was motivated by a large body of experimental and theoretical work (see [90] for references), it also meant that the base state was no longer steady but time-periodic. This has implications for the optimisation procedure which now not only has to search for the optimal initial perturbation but also the exact time (or phase) during the base flow period when it should be introduced.

### *4.4. Magnetic field generation*

[113] treats the kinematic dynamo problem looking for the velocity field of an electrically-conducting fluid which produces the greatest growth of magnetic field at the end of a time interval $T$. The set of competitor fields is constrained either by the total energy or the $L_2$ norm of their strain rate (or equivalently the viscous dissipation rate) only. By using the optimisation procedure described here, a lower bound on the magnetic Reynolds number is identified for a dynamo which is only a 1/5th of that possible within the well-studied ABC-class of flows [23, 1].

Finally, we close this section by noting that the optimisation procedure discussed in this article is closely related to the well known data assimilation procedure wherein a dynamical model of, and incomplete observations about, a real time-evolving system are used to constrain the initial state of the model such that the 'best' solution over a given time horizon can be sought. This is achieved by minimising an appropriate cost functional which penalises the deviations of the predicted solution away from known observations and possible uncertainties in the dynamical model. In contrast, the optimisation approach discussed here assumes a perfect dynamical model and seeks to maximise an objective functional over all initial conditions of a certain size in the absence of constraining observations. Data assimilation is used extensively in many areas of the geosciences (such as weather forecasting e.g [28, 56], oceanography [7] and more recently modelling the Earth's dynamo [42] ).

## 5. Final summary and future directions

This article has been a simple introduction to an optimisation technique which offers a new way to probe the basin boundary of a state in a dynamical system. Although the discussion has concentrated on this well-defined situation for clarity of exposition, the technique can also usefully be employed for systems with just one global attractor and

at least one long-lived but ultimately-repelling state (sheared fluid flows with enforced short wavelength dynamics are prime examples of this situation since then the turbulence seems only transient e.g. [38, 100]). Then the global attractor does not have a basin boundary but there is instead an 'edge' or manifold in phase space which divides initial conditions which immediately converge to the global attractor and those that first visit one of the repellors. The same game can then be played providing a functional can be identified which is clearly maximised in the target repellor for a time long enough for the repellor to be reached yet shorter than the mean lifetime of that repellor. This is in fact probably the situation in all the fluid flow calculations done so far (e.g. the turbulence in the 5 diameter long pipe in [87] is actually only transient at $Re = 2400$ but the mean lifetime is so large $\gg 100D/U$ that it mimicks an attractor on the timescales of the calculations).

The optimisation technique involves maximising a functional which takes on much larger values in the target state than in the basin of attraction of the starting state subject to an initial amplitude constraint and other constraints which include that the governing equations are satisfied - see the summary in §3.3. The iterative approach to solving this variational problem is not new or the realisation that there should be a sudden jump in the optimal value as the initial amplitude increases to penetrate the basin boundary particularly profound. What is noteworthy, however, is that the technique appears to work for large degree-of-freedom discretizations of PDE systems approaching practical application.

For the particular application studied here - transition to turbulence in shear flows - the optimisation approach provides a pleasing theoretical bridge between the two different theoretical perspectives of (linear) optimal perturbation theory and the (nonlinear) dynamical system approach. It is now much clearer how nonlinearity interacts with the linear transient growth mechanisms to achieve transition at least close to the amplitude threshold. Furtrhermore, the first steps have been taken to actively use the technique to *design* more stable states by adjusting their driving slightly [90].

There are practical issues, however, needing development. The optimisation techniques being used to maximise the objective function given gradient information with respect to the initial conditions are typically simple-minded with no attempt made so far to tailor them to the system being treated. There is also no consensus as yet on what convergence criteria should be used or *a posteriori* checks to confirm that the global maximum has been found. The last issue is particularly important of course and an agreed level of care is needed.

### *5.1. Future directions*

The optimisation approach is incredibly flexible and there is no reason why other information cannot be sought from a dynamical system. For example, [87] talks about identifying the peak instantaneous pressure in a transitional fluid flow, which is of key concern in certain applications (e.g. pipeline structural integrity). Also, so far,

only the basin boundaries of steady and time-periodic states have been probed using this technique. Demonstrating feasibility for a state with more exotic time-dependence remains to be done.

In terms of making greater connection with experiments, the competitor set of initial states can also be restricted to acknowledge the fact that only a reduced subset of all initial conditions are achievable in the laboratory. This can be accomplished simply by projecting the gradient vector of the objective functional onto a reduced set of realisable initial conditions and looking for the minimal seed in this subclass of disturbances. Looking to make contact with real systems also highlights a considerable simplification implicit in the discussion so far: the assumption has been that the system is disturbed *once* and then evolves perfectly. In practice, disturbances to real systems are not isolated or indeed equally likely. Developing the optimisation technique to encompass these realities will obviously be important. Some tentative steps have already been made by considering multiple discrete disturbances [66] and examining how adding noise to a system can still pick out the minimal seed route to 'transition' [112].

Hopefully, the power of the optimisation technique discussed here should be clear now. Ever increasing computer power is making direct simulations of systems more common with the concomitant need to process and interpret this data crucial. The optimisation technique discussed here has a huge potential to help with this and should surely become a standard theoretical tool in the near future.

*Acknowledgements*
EPSRC funding for Chris Pringle (and Sam Rabin?)

## Appendix A: The 2D linear transient growth problem

The dynamics in the simple ODE model (10) around the equilibrium $\mathbf{X}_0 = (0, 0)$ are linearised when $d \ll 1$. In this limit, the equation for $\mathbf{x}$ is just

$$\frac{d\mathbf{x}}{dt} = L\mathbf{x}, \quad \text{where} \quad L := \begin{bmatrix} -1 & 10 \\ 0 & -10 \end{bmatrix} \tag{44}$$

and standard matrix manipulations can then calculate the maximal achievable distance after a time $T$. $L$ has eigenvalues $\lambda_1 = -1$ and $\lambda_2 = -10$ and corresponding eigenvectors $\mathbf{q}_1$ and $\mathbf{q}_2$. Defining the matrix $\mathbf{Q} := (\mathbf{q}_1|\mathbf{q}_2)$ (the 2 eigenvectors arranged in columns)

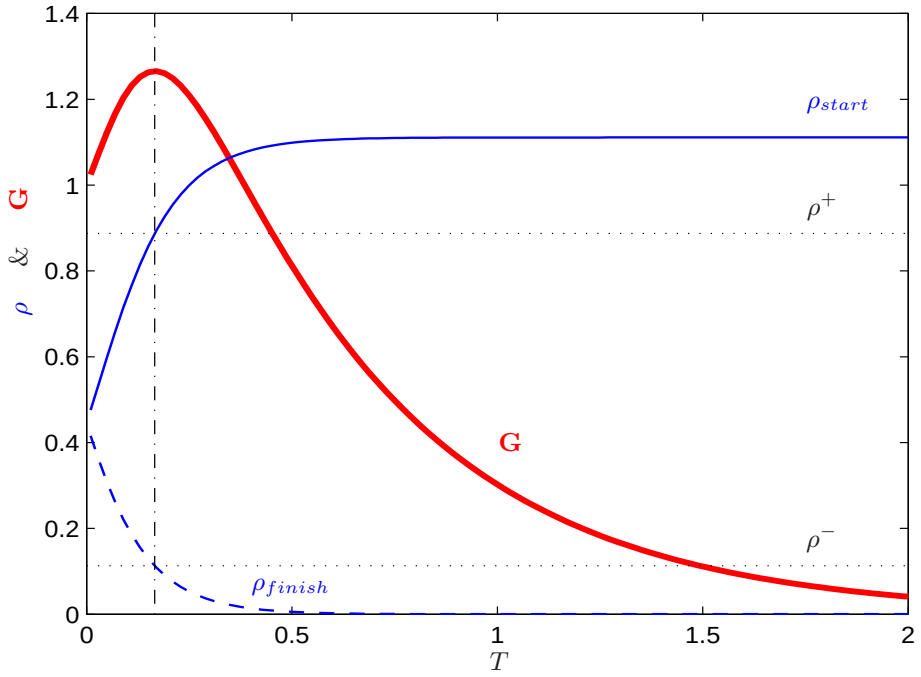


**Figure 8.** The maximum gain $G$ (thick red line) against target time $T$ for the linear system (44). The thinner solid/dashed blue lines indicate the starting/finishing values of $\rho := x_2/x_1$ for the corresponding optimal. Also shown as horizontal (black) dotted lines are the orientations where energy growth starts ($\rho^+$) and finishes ($\rho^-$ ) ($\rho$ decreases in time for $x_2(0) > 0$). Notice that the maximum growth occurs precisely when the initial condition has $\rho(0) = \rho^+$ *and* $T$ is such that $\rho(T) = \rho^-$.

and

$$e^{\mathbf{\Lambda} T} = \begin{bmatrix} e^{\lambda_1 T} & 0 \\ 0 & e^{\lambda_2 T} \end{bmatrix} \tag{45}$$

then, if $\mathbf{a}$ is a vector specifying the initial condition

$$\mathbf{x}(0) = \sum_{j=1}^{2} a_j \mathbf{q}_j = \mathbf{Q}\mathbf{a} \quad \Rightarrow \quad \mathbf{x}(t) = \sum_{j=1}^{2} a_j e^{\lambda_j T} \mathbf{q}_j = \mathbf{Q} e^{\mathbf{\Lambda} T} \mathbf{a}. \tag{46}$$

Then $\max \mathcal{L} := G\, d^2$ where the gain

$$G(T) = \max_{\mathbf{a}} \frac{\|\mathbf{x}(T)\|_2^2}{\|\mathbf{x}(0)\|_2^2} = \max_{\mathbf{a}} \frac{\mathbf{a}^\dagger e^{\mathbf{\Lambda} T} \mathbf{Q}^\dagger \mathbf{Q} e^{\mathbf{\Lambda} T} \mathbf{a}}{\mathbf{a}^\dagger \mathbf{Q}^\dagger \mathbf{Q} \mathbf{a}} = \|\mathbf{M}\|_2^2 \tag{47}$$

and $\mathbf{M} := \mathbf{Q} e^{\mathbf{\Lambda} T} \mathbf{Q}^{-1}$ ($^\dagger$ indicating transpose). $G$ is therefore the largest singular value of $\mathbf{M}$ or equivalently the largest (real) eigenvalue of the symmetric matrix $\mathbf{M}^\dagger \mathbf{M}$. The linear optimal $\theta = \theta^*$ increases monotonically from 0.1413 ($25.4^o$) at $T = 0$, through 0.2322 ($41.8^o$) at T=0.16615 where $G$ peaks at 1.26590, and then onto 0.2667 ($48.0^o$) where $G \to 0$ as $T \to \infty$: see figure 8.

In 2D, the situation is sufficiently simple to analyse completely for the general linear problem

$$\frac{d\mathbf{x}}{dt} = L\mathbf{x} := \begin{bmatrix} -a & b \\ 0 & -c \end{bmatrix} \mathbf{x} \tag{48}$$

with $a, b$ and c all positive real numbers (the interesting stable case). Defining $\rho(t)$ as the orientation $x_2(t)/x_1(t)$ and energy $E(t) := \frac{1}{2}\mathbf{x}(t)^2$, energy growth begins at the orientation $\rho^+$ and ends at the orientation $\rho^-$ where

$$\rho^{\pm} := \frac{b \pm \sqrt{b^2 - 4ac}}{2c}. \tag{49}$$

The eigenvalues of $L$ are $-a$ and $-c$ and with their corresponding eigenvectors, the general solution to (48) can be written down as

$$\mathbf{x}(t) = \alpha \begin{bmatrix} 1 \\ 0 \end{bmatrix} e^{-at} + \beta \begin{bmatrix} b/(a-c) \\ 1 \end{bmatrix} e^{-ct}. \tag{50}$$

Imposing the conditions that $\rho(0) = \rho^+$ and $\rho(T) = \rho^-$ requires

$$\frac{\beta}{\alpha} = \frac{\rho^+(c-a)}{c - a + b\rho^+}, \qquad T^* := \frac{1}{c-a} \log\Big[\left(\frac{\rho^+}{\rho^-}\right) \frac{c - a + b\rho^-}{c - a + b\rho^+}\Big] \tag{51}$$

so that

$$G_{\max} = \frac{\rho^{+2}(\rho^{-2}+1)}{\rho^{-2}(\rho^{+2}+1)} e^{-2cT^*}. \tag{52}$$

## Appendix B: Linear verses nonlinear transient growth

Here we discuss how nonlinear optimals are related to linear optimals when the nonlinearity in the system preserves the functional being optimised (a prime example being the energy-preserving nonlinearity of the Navier-Stokes equations in fluid mechanics). Consider an ODE system whose phase space is partitioned into subspaces each of which is invariant under the linearised dynamics about the origin $\mathbf{x} = \mathbf{0}$ which is a stable fixed point. If some of the subspaces support transient growth then it is possible for nonlinearities in the system to couple these growth processes to give much larger overall growth than any possible in the linearised dynamics. To illustrate this, we take a simple 4D system which has two such subspaces,

$$\dot{x} := \frac{d\mathbf{x}}{dt} = \begin{bmatrix} -a & b & 0 & 0 \\ 0 & -c & 0 & 0 \\ 0 & 0 & -\epsilon a & \epsilon b \\ 0 & 0 & 0 & -\epsilon c \end{bmatrix} \mathbf{x} + \begin{bmatrix} -x_1 x_4 \\ 0 \\ 0 \\ x_1^2 \end{bmatrix}. \tag{53}$$

For simplicity, the linear dynamics in each subspace are identical up a change in timescale which means that the same maximum transient growth ( $G_{\max}$ given by (52) ) occurs in each but at two different times (given by (51) ); $T^*$ for subspace $U_1 := \{(x_1, x_2, 0, 0) \,|\, x_1, x_2 \in \mathbb{R}\}$ and $T^*/\epsilon$ for subspace $U_2 := \{(0, 0, x_3, x_4) \,|\, x_3, x_4 \in \mathbb{R}\}$:

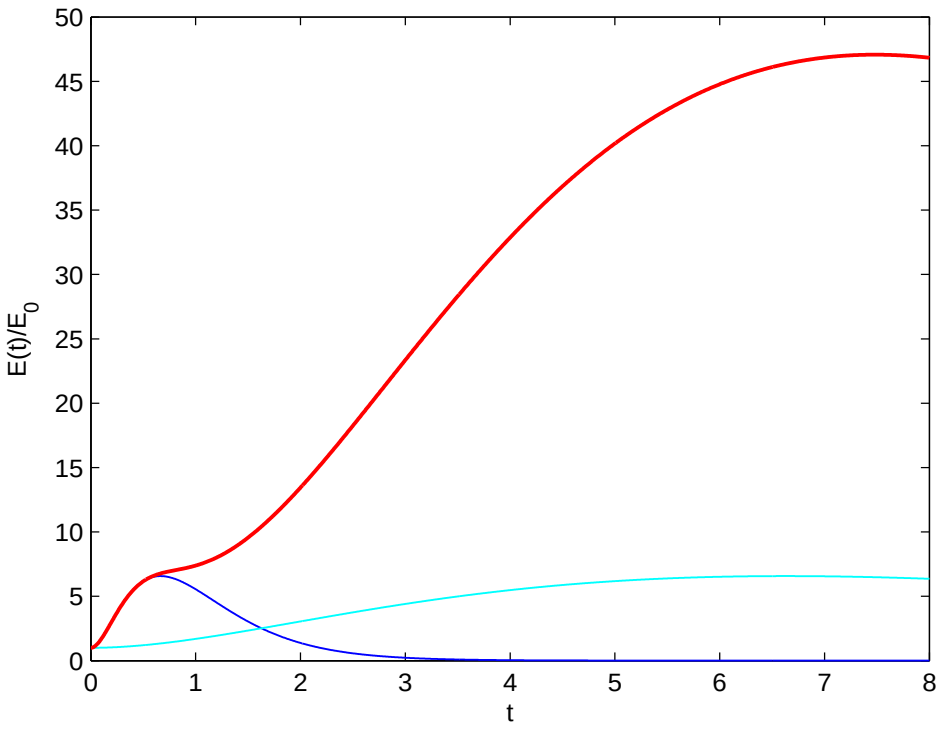


**Figure 9.** Linear and nonlinear transient growth for the system (53) with $(a, b, c, \epsilon) = (1, 10, 2, 0.1)$. The thin blue and cyan lines show optimal growth in $U_1$ and $U_2$ which both have a peak gain $G$ of 6.57 but at different times $T^* = 0.66$ and $T^*/\epsilon$ respectively for infinitesimally small initial energies. The thick red line is the result of using the optimal initial condition (54) for the $U_1$ with $\delta = 0.15$ which is sufficient to allow the two transient growth processes to combine to produce much larger overall growth. Note the similarity of this nonlinear curve to that in figure 5.

see Figure 9. Minimal nonlinear terms are included designed to a) conserve energy (as in the Navier-Stokes equations) and b) to allow the faster energy growth in subspace $U_1$ to pump-prime the slower growth in subspace $U_2$. This is clearly seen to occur for $\delta$ large enough when taking the optimal initial condition for $U_1$

$$\mathbf{x}(0) = (x_1, x_2, x_3, x_4) = \delta(1, \rho^+, 0, 0), \tag{54}$$

see Figure 9 for an example using $(a, b, c, \epsilon) = (1, 10, 2, 0.1)$ (for the linear problem in $U_1$, $G_{\max} = 6.57$ and $T^* = 0.66$).

If the terms 'LOP' and 'NLOP' indicate the global linear and nonlinear optimals over asymptotically large $T$, both clearly must have

$$\dot{E}(0) = 0 \tag{55}$$

($E := \frac{1}{2}\mathbf{x}^2$) otherwise the time origin could be adjusted to increase the overall growth [25]. Since $\dot{E}$ is only determined by the linear terms (the nonlinear terms can't contribute as they are energy-preserving), then all the candidate initial conditions satisfying the

constraint $\dot{E} = 0$ for the full nonlinear optimisation problem are actually present in the linear problem. However, the linear problem may never select the NLOP for *any* $T$ because without nonlinearity its growth is overshadowed by other candidates (i.e. the NLOP would be only be a local rather than global maximum). To illustrate this with a concrete example, consider a 6D extension of the above 4D system by adding another 2D subspace $U_3$ to $U_1 \bigoplus U_2$. If the linear transient growth in $U_3$ always produces slightly more growth over any choice of $T$ than $U_1$ (at least until the slower growth in $U_2$ takes over), the linear optimisation problem will never select any candidate initial condition which has some projection in $U_1$. In contrast the NLOP will be the linear optimal for $U_1$ (i.e. (54) ) since this is the only way $\dot{E}(0)$ vanishes non-trivially in $U_1$. This situation is borne out by the NLOP found in (very high dimensional) pipe flow [86, 87]. In just 2D, however, there are only two candidates in the linear problem which are joint global optimisers. Hence in this case the NLOP has to be contained in the linear problem trivially.

## References


[1] Alexakis A 2011 Searching for the fastest dynamo: laminar ABC flows *Phys. Rev. E* **84** 026321.

[2] Andersson P, Berggren M and Henningson D S 1999 Optimal disturbances and bypass transition in boundary layers *Phys. Fluids* **11** 134-150.

[3] Babloyantz A and Destexhe A 1986 A low-dimensional chaos in an instance of epilepsy *Proc. Natl. Acad. Sci.* **83** 3513-3517

[4] Baggett J S and Trefethen L N 1995 Low-dimensional models of subcritical transition to turbulence *Phys. Fluids* **9** 1043-1053.

[5] Baggett J S, Driscoll T A and Trefethen L N 1997 A mostly linear-model of transition to turbulence *Phys. Fluids* **7** 833-838.

[6] Barkmeijer J 1996 Constructing fast-growing perturbations for the nonlinear regime *J. Atmos. Sci.* **53** 2838-2851.

[7] Bennett A F 1992 *Inverse Methods in Physical Oceanography* Cambridge University Press.

[8] Berggren M 1998 Numerical solution of a flow-control problem: vorticity reduction by dynamic boundary action *Siam J. Sci. Comput.* **19** 829-860.

[9] Bewley T R, Moin P and Temam R 2001 DNS-based predictive control of turbulence: an optimal benchmark for feedback algorithms *J. Fluid Mech.* **447** 179-225.

[10] Biau D and Bottaro A 2004 Transient growth and minimal defects: two possible initial paths of transition to turbulence in plane shear flows *Phys. Fluids* **16** 3515-3529.

[11] Biau D and Bottaro A 2009 An optimal path to transition in a duct *Phil. Trans. Roy. Soc. Lond.* **A 367** 529-544.

[12] Boberg L and Brosa U 1988 Onset of turbulence in a pipe *Z. Naturforsch.* **43a** 697-726.

[13] Bottaro A, Corbett P and Luchini P 2003 The effect of base flow variationon flow instability *J. Fluid Mech.* **596** 113-142.

[14] Buizza R and Palmer T N 1995 The singular-vectorstructure of the atmospheric global circulation *J. Atmos. Sci.* **52** 1434-1456.

[15] Butler K M and Farrell B F 1992 3-Dimensional optmal perturbations in viscous shear-flow *Phys. Fluids* **4** 1637-1650.

[16] Cantwell C D, Barkley D and Blackburn H M 2010 Transient growth analysis of flow through a sudden expansion in a circular pipe *Phys. Fluids* **22** 034101.

[17] Chandrasekhar S 1961 *Hydrodynamic and Hydromagnetic Instability*, Oxford University Press.

[18] Cherubini S, De Palma P, Robinet J-C and Bottaro A 2010 Rapid path to transition via nonlinear localised optimal perturbations in a boundary layer flow *Phys. Rev. E* **82** 066302.
[19] Cherubini S, De Palma P, Robinet J-C and Bottaro A 2011 The minimal seed of turbulent transition in the boundary layer *J. Fluid Mech.* **689** 221-253.
[20] Cherubini S, De Palma P, Robinet J-C and Bottaro A 2012 A purely nonlinear route to transition approaching the edge of chaos in a boundary layer *Fluid Dynam. Res.* **44** 031404 (11 pages).
[21] Cherubini S and De Palma P 2013 Nonlinear optimal perturbations in a Couette flow: bursting and transition *J. Fluid Mech.* **716** 251-279.
[22] Cherubini S, Robinet J-C and De Palma P 2013 Nonlinear control of unsteady finite-amplitude perturbations in the Blasius boundary-layer flow *J. Fluid Mech.* **737** 440-465
[23] Childress S 1970 New solutions of the kinematic dynamo problem *J. Math Phys.* **11** 3063-3076
[24] Corbett P and Bottaro A 2000 Optimal perturbations for boundary layers subject to streamwise pressure gradient *Phys. Fluids* **12** 120-130.
[25] Cossu C 2005 An optimality condition on the minimum energy threshold in subcritical instabilities *C. R. Mecanique* **333** 331-336.
[26] Cvitanović P and Gibson J F 2010 Geometry of turbulence in wall-bounded shear flows: periodic orbits *Phys. Scr.* **142** 014007.
[27] Dauchot O and Manneville P 1997 Local versus global concepts in hydrodynamic stability theory *J. Phys. II France* **7** 371-389.
[28] Daley R 1991 *Atmospheric data analysis* Cambridge University Press.
[29] Drazin P G 2002 *Introduction to Hydrodynamic Stability* Cambridge University Press.
[30] Drazin P G and Reid W H 1981 *Hydrodynamic Stability* Cambridge University Press.
[31] Duan W and Zhou F 2013 Non-linear forcing singular vector of a two-dimensional quasi-geostrophic model *Tellus* **65** 18452.
[32] Duguet Y, Brandt L and Larsson B R J 2010 Towards minimal perturbations in transitional plane Couette flow *Phys. Rev. E* **82** 026316 (13 pages).
[33] Duguet Y, Monokrousos A, Brandt L and Henningson D S 2013 Minimal transition thresholds in plane Couette flow *Phys. Fluids* **25** 084103 (23 pages).
[34] Eckhardt B, Faisst H, Schmeigel A and Schumacher J 2002 Turbulence transition in shear flows. *Advances in Turbulence IX: Proceedings 9th European Turbulence Conference* (Southampton) (ed. I. P. Castro et al.), p701, CISME.
[35] Eckhardt B, Schneider T M, Hof B and Westerweel J 2007 Turbulence transition in pipe flow *Ann. Rev. Fluid Mech.* **39** 447-468.
[36] Ellingsen T and Palm E 1975 Stability of linear flow *Phys. Fluids* **18** 487-.
[37] Ergäber H, Lenstra D, Krauskopf B, Wille E, Peil M, Fischer I and Elsasser W 2005 Mutually delay-coupled semiconductor lasers: Mode bifurcation scenarios *Opt. Commun.* **255** 286-296.
[38] Faisst H and Eckhardt B 2004 Sensitive dependence on initial conditions in transition to turbulence in pipe flow *J. Fluid Mech.* **504** 343-352.
[39] Farrell B F 1988 Optimal excitation of perturbations in viscous shear flow *Phys. Fluids* **31** 2093-2101.
[40] Farrell B F 1989 Optimal excitation of baroclinic waves *J. Atmos. Sci.* **46** 1193-1206.
[41] Farrell B F 1990 Small error dynamics and the predicability of atmospheric flows *J. Atmos. Sci.* **47** 2409-2416.
[42] Fournier A, Hulot G, Jault D, Kuang W, Tangborn A, Gillet N, Canet E, Aubert J and Lhuillier F 2010 An introduction to data assimilation and predictability in geomagnetism *Space Sci. Rev.* **155** 247-291.
[43] Gad-el-Hak M 2000 *Flow Control: Passive, Active and Reactive Flow Management*, Cambridge.
[44] Gavarini M I, Bottaro A and Nieuwstadt F T M 2004 The initial stage fo transition in pipe flow: rle of optimal base-flow distortions *J. Fluid Mech.* **517** 131-165.
[45] Gibson J F, Halcrow J and Cvitanović P 2008 Visualizing the geometry of state space in plane Couette flow *J. Fluid Mech.* **611**, 107-130.

[46] Grossmann S 2000 The onset of shear flow turbulence *Rev. Mod. Phys.* **72** 603-618.
[47] Guégan A, Schmid P J and Huerre P 2006 Optimal energy growth and optimal control in swept Hiemenz flow *J. Fluid Mech.* **566** 11-45.
[48] Gustavsson L H 1991 Energy growth of 3-dimensional disturbances in plane Poiseuille flow *J. Fluid Mech.* **224** 241-260.
[49] Heisenberg W 1924 Über stabilität und turbulenz von flussigkeitsströmen *Ann. Phys. Lpz.* **74** 577-627.
[50] Hinze M, Walther A and Sternberg J 2006 An optimal memory-reduced procedure for calculating adjoints of the instationary Navier-Stokes equations *Optim. Control Appl. Methods* **27** 19-40.
[51] Hopf E 1948 A mathematical example displaying features of turbulence *Commun. Appl. Maths* **1**, 303-322.
[52] Hultgren L S and Gustavsson L H 1981 Algebraic growth of disturbances in a laminar boundary-layer *Phys. Fluids* **24** 1000-1004.
[53] Itano T and Toh S 2001 The dynamics of bursting process in wall turbulence *J. Phys. Soc. Japan* **70** 703-716.
[54] Jegadeesan V and Sujith R I 2013 Experimental investigation of noise induced triggering in thermoacoustic systems *Proceedings of the Combustion Institute* **34** 3175-3183.
[55] Jiang Z N, Mu M and Luo D H 2013 A study of the North Atlantic Oscillation using conditional nonlinear optimal perturbation *J. Atmos. Sci.* **70** 855-875.
[56] Kalnay E 2003 *Atmospheric Modelling, Data Assimilation and Predictability* Cambridge University Press.
[57] Kawahara G, Uhlmann M and van Veen L 2012 The significance of simple invariant solutions in turbulent flows *Ann. Rev. Fluid Mech.* **44** 203-225.
[58] Kerswell R R 2005 Recent progress in understanding the transition to turbuelnce in a pipe *Nonlinearity* **18** R17-R44.
[59] Kerswell R R 2011 Lecture 9: Triggering Transitions - Towards Minimal Seeds, *Summer program in Geophysical Fluid Dynamics*, Woods Hole Oceanographic Institute, Massachusetts, USA (http://www.whoi.edu/main//gfd/proceedings-volumes/2011)
[60] Kim J and Bewley T R 2007 A linear systems approach to flow control *Ann. Rev. Fluid Mech.* **39** 383-417.
[61] Kitson S and Geisow A 2002 Controllable alignment of nemantic liquid crystals around microscopic posts: stabilization of multiple states *Appl. Phys. Lett.* **80** 3635-3637.
[62] Juniper M P 2011 Triggering in the horizontal Rijke tube: non-normality, transient growth and bypass transition *J. Fluid Mech.* **667** 272-308
[63] Juniper M P 2011 Transient growth and triggering in the horizontal Rijke tube *Int. J. Spray and Combustion Dynamics* **3** 209-224.
[64] Landahl M T 1980 A note on an algebraic instability of inviscid parallel shear flows *J. Fluid Mech.* **98** 243-.
[65] Landau L D 1944 On the problem of turbulence *C.R. Acad. Sci. U.R.S.S.* **44** 311-314.
[66] Lecoanet D and Kerswell R 2013 Nonlinear optimization of multiple perturbations and stochastic forcing of subcritical ODE systems *Bull. Am. Phys. Soc.* **58** http://meetings.aps.org/link/BAPS.2013.DFD.L10.4
[67] Lorenz E N 1965 A study of the predicability of a 28-variable atmosphere model *Tellus* **17** 321-333.
[68] Luchini P and Bottaro A 1998 Görtler vortices: a backward-in-time approach to the receptivity problem *J. Fluid Mech.* **363** 1-23.
[69] Luchini P 2000 Reynolds-number-independent instability of the boundary layer over a flat surface: optimal perturbations *J. Fluid Mech.* **404** 289-309
[70] Luchini P and Bottaro A 2014 Adjoint equations in stability analysis *Ann. Rev. Fluid Mech.* **46** 493-517.
[71] Machowski J, Bialek J W and Bumby J R 2008 *Power System Dynamics: Stability and Control*, Wiley.

[72] Menck P J, Heitzig J, Marwan N and Kurths J 2013 How basin stability complements the linear-stability paradigm *Nature Phys.* **9** 89-92.
[73] Monokrousos A, Bottaro A, Brandt L, Di Vita A and Henningson D S 2011 Nonequilibrium thermodynamics and the optimal path to turbulence in shear flows *Phys. Rev. Lett.* **106** 134502.
[74] Mu M 2000 Nonlinear singular vectors and nonlinear singular values *Sci. China* **43D** 375-385.
[75] Mu M, Duan W S and Wang B 2003 Conditional nonlinear optimal perturbation and its applications *Nonlin. Processes Geophys.* **10** 493-501.
[76] Mu M, Sun L and Dijstra H A 2004 The sensitivity and stability of the ocean's thermohaline circulation to finite-amplitude perturbations *J. Phys. Ocean.* **34** 2305-2315.
[77] Mu M and Zhang Z 2006 Conditional nonlinear optimal perturbations of a two-dimensional quasigeostrophic model *J. Atmos. Sci.* **63** 1587-1604.
[78] Mu M and Jiang Z N 2008 A new approach to the generation of initial perturbations for ensemble prediction using dynamically conditional perturbations *Chinese Sci. Bull.* **53**, 2062-2068.
[79] Mu M and Jiang Z 2008 A method to find perturbations that trigger blocking onset: conditional nonlinear optimal perturbations *Am. Meteor. Soc.* **65** 3935-3946.
[80] Mullin T 2011 Experimental Stuides of Transition to Turbulence in a Pipe *Ann. Rev. Fluid Mech.* **43** 1-24.
[81] Noether F 1921 Das turbulenz problem *Z. angew. Math. Mech.* **1** 125-138.
[82] Oortwijn J and Barkmeijer J 1995 Perturbations that optimally trigger weather regimes *J. Atmos. Sci.* **52** 3932-3944.
[83] Orr W M 1907 The stability or instability of the steady motions of a perfect fluid and of a viscous fluid. Part I. A perfect fluid. Part II A viscous fluid *Proc. Roy. Irish Acad.* **27** 9-138.
[84] Palmer T, Molteni F, Mureau R, Buizza R, Chapelet P and Tribbia J 1993 Ensemble prediction *Proc. ECMWF Seminar* **1** Reading, UK ECMWF 21-66.
[85] Passaggia P-Y and Ehrenstein U 2013 Adjoint based optimisation and control of a separated boundary-layer flow *Eur. J. Mech. B* **41** 169-177.
[86] Pringle C C T and Kerswell R R 2010 Using nonlinear transient growth to construct the minimal seed for shear flow turbulence *Phys. Rev. Lett.* **105** 154502.
[87] Pringle C C T, Willis A P and Kerswell R R 2012 Minimal seeds for shear flow turbulence: using nonlinear transient growth to touch the edge of chaos *J. Fluid Mech.* **702** 415-443.
[88] Pringle C C T, Willis A P and Kerswell R R 2014 Streamwise localised nonlinear energy optimals *Phys. Fluids* in preparation
[89] Rabin S M E, Caulfield C P and Kerswell R R 2012 Variational identification of minimal seeds to trigger transition in plane Couette flow *J. Fluid Mech.* **712** 244-272.
[90] Rabin S M E, Caulfield C P and Kerswell R R 2014 Designing a more nonlinearly stable laminar flow via boundary manipulation *J. Fluid Mech.* **738** R1.
[91] Rayleigh Lord 1880 On the stability, or instability, of certian fluid motions *Proc. London Math. Soc.* **11** 57-70.
[92] Reddy S C and Henningson D S 1993 Energy growth in viscous channel flows *J. Fluid Mech.* **252** 209-238.
[93] Reddy S C, Schmid P J, Baggett J S and Henningson D S 1998 On stability of streamwise streaks and transition thresholds in plane channel flows *J. Fluid Mech.* **365** 269-303.
[94] Reshotko E 2001 Transient growth: a factor in bypass transition *Phys. Fluids* bf 13 1067-1075.
[95] Reynolds O 1883a An experimental investigation of the circumstances which determine whether the motion of water shall be direct or sinuous and of the law of resistance in parallel channels *Proc. R. Soc. Lond. Ser. A* **35** 84-99.
[96] Reynolds 0 1883b An experimental investigation of the circumstances which determine whether the motion of water shall be direct or sinuous and of the law of resistance in parallel channels *Phil. Trans. R. Soc. Lond. Ser. A* **174** 935-982.
[97] Schmid P J 2007 Nonmodal Stability Theory *Ann. Rev. Fluid Mech.* **39**, 129-62.
[98] Schmid P J and Henningson D S 2001 *Stability and Transition in Shear Flows* Springer-Verlag,

New York.

[99] Schneider T M, Eckhardt B and Yorke J A 2007 Turbulence transition and the edge of chaos in pipe flow *Phys. Rev. Lett.* **99** 034502.

[100] Schneider T M, De Lillo F, Buerhrle J, Eckhardt B, Dornemann T, Dornemann K, Freisleben B 2010 Transient turbulence in plane Couette flow *Phys. Rev. E* **81** 015301.

[101] Skufca J D, Yorke J A and Eckhardt B 2006 Edge of chaos in a parallel shear flow *Phys. Rev. Lett.* **96** 174101.

[102] Sommerfeld A 1908 Ein Beitrag zur hydrodynamischen erklaerung der turbulenten Fluessigkeitsbewegungen *Proceedings 4th International Congress of Mathematicians* Rome **III** 116-124.

[103] Taylor G I Stability of a viscous liquid contained between two rotating cylinders *Phil. Trans. Roy. Soc. Lond.* **223** 289-343.

[104] Terwisscha van Scheltinga A D and Dijkstra H A 2008 Conditional nonlinear optimal perturbations of the double-gyre ocean circulation *Nonlin. Processes Geophys.* **15** 727-734.

[105] Thomson W (Lord Kelvin) 1887 Stability of fluid motion - rectilineal motion of viscous fluid between two parallel plates *Philos. Mag.* **24** 188-.

[106] Toth Z and Kalnay E 1993 Ensemble forecasting at NMC: The generation of perturbations *Bull. Amer. Meteor. Soc.* **74**, 2317-2330.

[107] Toth Z and Kalnay E 1997 Ensemble forecasting at NCEP and the breeding method *Am. Meteor. Soc.* **125** 5297-3319.

[108] Trefethen L N, Trefethen A E, Reddy S C and Driscoll T A 1993 Hydrodynamic stability without eigenvalues *Science* **261** 578-584.

[109] Trefethen L N and Embree M 2005 *Spectra and Pseudospectra* Princeton Uuniversity Press.

[110] Viswanath D and Cvitanović P 2009 Stable manifolds and the transition to turbulence in pipe flow *J. Fluid Mech.* **627** 215-233.

[111] Waleffe F 1995 Transition in shear flows: nonlinear normality versus non-normal linearity *Phys. Fluids* **7** 3060-3066.

[112] Waugh I C and Juniper M P 2011 Triggering in a thermoacoustic system with stochastic noise *Int. J. Spray and Combustion Dynamics* **3** 225-242.

[113] Willis A P 2012 On the optimised magnetic dynamo *Phys. Rev. Lett.* **109** 251101.

[114] Zikanov O Y 1996 On the instability of pipe Poiseuille flow *Phys. Fluids* **8** 2923-2932.

[115] Ziqing Z U, Mu M and Dijkstra H A 2013 Optimal nonlinear excitation of decadal variability of the North Atlantic thermohaline circulation *Chinese J. Ocean. Limnology* **31** 1356-1362.

[116] Zuccher S, Luchini P and Bottaro A 2004 Algebraic growth in a Blasius boundary layer: optimal and robust control by mean suction in the nonlinear regime *J. Fluid Mech.* **513** 135-160.